Chapter 6
ELECTRON TRANSPORT

P. B. Allen

1. INTRODUCTION

A voltage gradient ($-\nabla\Phi = \mathbf{E}$) drives an electron current ($\mathbf{j} = \sigma\mathbf{E}$, where σ is the conductivity). Many mechanisms of electron transport are known.

(1) Electronic quasiparticle propagation, the first known mechanism, studied by Drude [1], and improved by Sommerfeld [2,3], Bloch [4], Landau [5], and others. The current is given by

$$\mathbf{j} = -\frac{e}{V}\sum_{k}\mathbf{v}_k F(k) \qquad (1)$$

where $F(k)$ is the distribution function (i.e. the non-equilibrium occupation) of the quasiparticle state k (short for: $\mathbf{k}, n, \sigma$) which has energy ε_k and group velocity $\mathbf{v}_k = \partial\varepsilon_k/\partial(\hbar\mathbf{k})$, and V the sample volume.
(2) Quasiparticle tunneling through barriers.
(3) Supercurrent flow in superconductors. The (Landau–Ginzburg) order parameter is $\psi = \sqrt{n_S}\exp(i\phi)$, and the current, with no magnetic field, is

$$\mathbf{j}_S = -\frac{(2e)\hbar}{2mi}(\psi^*\nabla\psi - \psi\nabla\psi^*) = -2en_S\hbar\nabla\phi/m \qquad (2)$$

where it is assumed that the superfluid density n_S is spatially uniform.
(4) Intrinsically diffusive currents in dirty alloys, metallic glasses, etc.
(5) Hopping currents in dilute electron systems where states are localized by (i) trapping at localized defects, (ii) Anderson localization at band tails in disordered media, or (iii) polaronic self-trapping in insulators.

(6) Separate propagation of charge and spin in 1D metals ("Luttinger liquids").
(7) Collective sliding of charge-density waves when incommensurate distortions open a gap in a metal.

This article will focus on examples where mechanisms can be clearly identified. Two other constraints are imposed. First, magnetic field effects (Hall effect, magneto-resistance, etc.) are excluded, for no good reason except to allow room for other things. Second, if an effect (like Anderson localization, or "weak localization") occurs in 3d bulk materials, and occurs in lower dimension in altered form, then only the 3d version is included here, for the same reason.

Transport is a subject of greater breadth and depth than can be covered in any one volume, let alone chapter. Thanks first to "mesoscopic" physics, and now, to "nanoscience," the field of transport is rapidly expanding and evolving. This chapter has three aims. First, to illustrate the breadth and beauty of the subject. Second, to illustrate how techniques from electronic structure theory are used to explain or predict values of transport coefficients such as electrical resistivity. Third, to guide a reader through some of the theoretical notions currently evolving as nanoscale research changes the way we think about these things.

2. CONDUCTIVITY

The conductivity σ is the usual starting point. Let there be an electric field varying slowly in space and sinusoidally in time, $\mathbf{E}(t) = \mathbf{E}\cos(\omega t)$. Then a bulk solid will respond to first order with an electrical current

$$j_\alpha(t) = \sigma_{\alpha\beta}^{(1)} E_\beta \cos(\omega t) + \sigma_{\alpha\beta}^{(2)} E_\beta \sin(\omega t) \tag{3}$$

To simplify, the tensor notation $\sigma_{\alpha\beta}$ will often be condensed to σ with implicit rather than explicit tensor aspects. Equation (3) is equivalent to $j(t) = \mathrm{Re}\left[\sigma(\omega)E\mathrm{e}^{-\mathrm{i}\omega t}\right]$, with a complex conductivity $\sigma = \sigma^{(1)} + \mathrm{i}\sigma^{(2)}$ whose real and imaginary parts denote in-phase (dissipative) and out-of-phase (reactive) response to the E field. I will use the standard Fourier conventions

$$E(t) = \int_{-\infty}^{\infty} \frac{\mathrm{d}\omega}{2\pi} E(\omega)\mathrm{e}^{-\mathrm{i}\omega t} \quad \text{and} \quad E(\omega) = \int_{-\infty}^{\infty} \mathrm{d}t E(t)\mathrm{e}^{\mathrm{i}\omega t} \tag{4}$$

to relate time to frequency; $j(t)$ and $\sigma(t)$ have the same connection to $j(\omega)$ and $\sigma(\omega)$. Since $j(t)$ and $E(t)$ are real, and since $j(\omega) = \sigma(\omega)E(\omega)$, it is necessary that $E(\omega)$ obey $E(-\omega) = E^*(\omega)$ and similarly for $j(\omega)$ and $\sigma(\omega)$.

The time-domain relation between j and E is

$$j(t) = \int_{-\infty}^{\infty} \mathrm{d}t' \sigma(t - t')E(t') \tag{5}$$

Thus, $\sigma(t)$ has the meaning that it gives the current at time t in response to an impulsive unit E-field $E(t') = \delta(t')$. "Causality" is the statement that if $E(t)$ is zero until it is "turned on" at time $t = 0$, then $j(t)$ must also be zero for times $t < 0$. Thus

$\sigma(t)$ must vanish for negative t, from which the Fourier relation Eq. (4) becomes $\sigma(\omega) = \int_0^\infty \mathrm{d}t\sigma(t)\exp(i\omega t)$. Now let us regard $\sigma(\omega)$ as a function of a complex ω. When $\mathrm{Im}[\omega]>0$ (that is, in the upper half ω-plane) the integral converges absolutely, permitting interchange of derivative and integral from which follows $\partial\sigma_1/\partial\omega_1 = \partial\sigma_2/\partial\omega_2$ and $\partial\sigma_1/\partial\omega_2 = -\partial\sigma_2/\partial\omega_1$. These are the Cauchy–Riemann equations which confirm that $\sigma(\omega)$ is analytic in the upper-half ω-plane. This is the basis for the Kramers–Kronig integral relations between real and imaginary part of $\sigma(\omega)$ for real ω.

Consider the Drude formula [1], originally proposed on classical grounds, for the conductivity of metals:

$$\sigma_{\mathrm{Drude}}(\omega) = \frac{ie^2(n/m)_{\mathrm{eff}}}{\omega + i/\tau} \tag{6}$$

The factor $(n/m)_{\mathrm{eff}}$ is discussed later, see Eqs. (26) and (55). For simple metals, $(n/m)_{\mathrm{eff}}$ is fairly close to n/m, where n is the valence electron density and m the free electron mass. The electron charge is $-e$. Unlike these parameters with fixed classical meaning, τ is a phenomenological parameter indicating the time between the collision events which allow electrons to reach a steady-state current. Note that $\sigma(\omega)$ has a pole at $\omega = -i/\tau$, that is, in the lower part of the complex ω-plane. By Fourier inversion we find

$$\sigma_{\mathrm{Drude}}(t) = e^2\left(\frac{n}{m}\right)_{\mathrm{eff}} e^{-t/\tau}\theta(t) \tag{7}$$

where $\theta(t)$ is the unit step function, zero for $t<0$ and 1 for $t>0$. The real part of $\sigma(\omega)$ is a Lorentzian, with conserved spectral weight

$$\int_{-\infty}^\infty \mathrm{d}\omega\sigma_{\mathrm{Drude}}^{(1)}(\omega) = \pi e^2\left(\frac{n}{m}\right)_{\mathrm{eff}} \quad \text{but} \quad \int_{-\infty}^\infty \mathrm{d}\omega\sigma_{\mathrm{exact}}^{(1)}(\omega) = \pi e^2\left(\frac{n_{\mathrm{total}}}{m}\right) \tag{8}$$

Both of these are unaffected by the phenomenological parameter τ. The second version, for the *exact* σ, is the "f-sum rule." It is equivalent to the statement that $\sigma(t = 0^+)$, which is the current just after a unit pulse $E(t) = \delta(t)$ has been applied, is given by the classical constant $n_{\mathrm{total}}e^2/m$, where n_{total} includes core as well as valence electrons, and the integral includes ultraviolet and x-ray regions of the spectrum. In the limit of an infinitely sharp pulse and zero elapsed time, electrons have not yet responded to anything other than the E-field. They do not notice the positive nuclei or the Coulomb repulsion with each other. Thus the sum rule is true for any system, molecule or extended, insulator or metal, crystal or glass.

Now consider the experimental results [6] for copper, the prototype ordinary metal, shown in Fig. 1. The dielectric "constant" $\varepsilon(\omega)$ is defined by $\varepsilon = 1 + 4\pi P/E$ where the polarization P is related to current j by $j = \partial P/\partial t$. Therefore, we have $\varepsilon(\omega) = 1 + 4\pi i\sigma(\omega)/\omega$, and $\varepsilon^{(2)} = 4\pi\sigma^{(1)}/\omega$. The Drude Lorentzian, centered at $\omega = 0$, has a strength measured in terms of the "Drude plasma frequency" $\omega_{\mathrm{P}}^2 = 4\pi e^2(n/m)_{\mathrm{eff}}$. Theory [7] gives $\hbar\omega_{\mathrm{P}} = 9.1\,\mathrm{eV}$. This can be compared with the free electron value, $10.8\,\mathrm{eV}$, which is based on a simplified model of 1 rather than 11 valence electrons per Cu atom. The Drude part of $\sigma(\omega)$ becomes quite small for
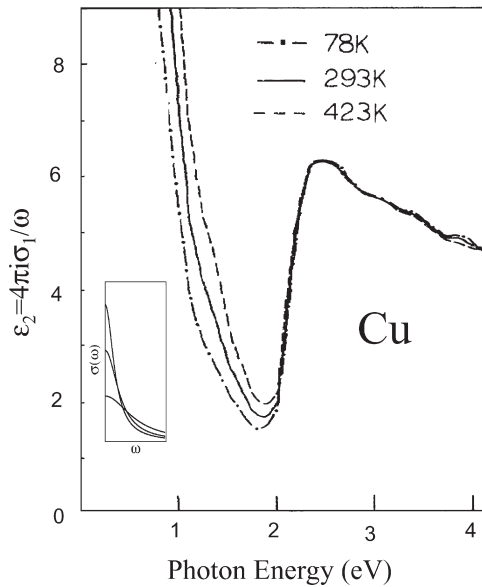
Fig. 1. Measured optical properties of Cu metal at three temperatures [6]. Interband transitions set in above 2 eV. At lower frequencies, the tail of the Drude part varies with temperature. The inset is a schematic of the real part of the Drude conductivity $\sigma(\omega)$, Eq. (6) at three temperatures.

photon energies $\hbar\omega$ as high as 2 eV. At higher photon energies, σ_1 increases, indicating additional non-Drude currents, which are caused by electrons making quantum transitions from d-states not far below the Fermi energy E_F into s-states above the Fermi energy, with a conserved wavevector **k**. The f-sum Eq. (8) is approximately divided into spectral weight in the Drude region below 2 eV, and spectral weight from interband transitions. As temperature T changes, the spectral weight in the Drude region is conserved. The formula for $(n/m)_{eff}$ needs a treatment of the energy bands, discussed in Section 4.2 from a quantum approach, and then discussed again from a semiclassical point of view in Section 6.2. Although the interband part of $\sigma(\omega)$ is normally classified as "optical properties" rather than "transport," nevertheless, there is no truly fundamental distinction, and understanding of low-ω transport requires some understanding of high-ω behavior.

3. CONDUCTANCE *VERSUS* CONDUCTIVITY: THE POINT CONTACT

For homogeneous bulk matter, the electrical properties are characterized by the intrinsic conductivity $\sigma = 1/\rho$ of the material. For other cases, conductance $G = 1/R$ is the appropriate parameter. Figure 2 illustrates the reason.
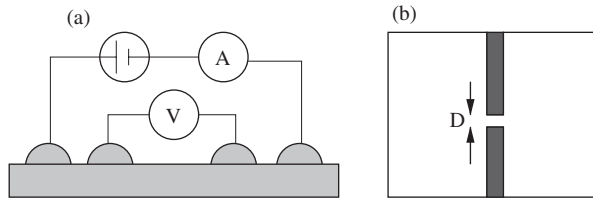
Fig. 2. (a) The usual four probe geometry for measuring resistivity of a bulk material. The voltmeter draws negligible current and thus does not disturb the electrical potential distribution. (b) An idealized orifice of diameter D in an otherwise bulk sample. For D small compared with the sample dimensions, the resistance is dominated by the alteration of electrical potential in the vicinity of the orifice. This is a model for a "point contact."

In the usual bulk case, the conductance is $G = \sigma A/L$ where σ is an intrinsic property, A the cross-sectional area of the conductor, and L the length. But in panel (b) of Fig. 2 (a model for a "point contact"), the conductance is limited by the orifice of diameter D. The spatial variation of the potential $V(\mathbf{r})$ must be solved self-consistently. Maxwell [8] solved this problem under the assumption of a local relation $\mathbf{j}(\mathbf{r}) = \sigma \mathbf{E}(\mathbf{r})$ between current and field, where σ is the conductivity of the homogeneous "bulk" material. He obtained $G_{\mathrm{M}} = D\sigma$. The resistance $R_{\mathrm{M}} = 1/D\sigma$ is dominated by the constriction; the remainder (the "electrodes") adds a series resistance $R = L/A\sigma \ll 1/D\sigma)$ which vanishes in the limit of large dimensions $L \gg D$ and $A/L \gg D$. In such a case, the conductivity does not describe transport through the system and it is necessary to study conductance.

The local relation assumed by Maxwell holds when the mean electron free path ℓ (equal to $v_{\mathrm{F}}\tau$ where v_{F} is an average Fermi velocity) is small compared to the diameter D of the constriction. The problem becomes more interesting in the opposite limit. Because of the long mean-free path, the current at point $\mathbf{r}$ depends on the $\mathbf{E}$-field at points $\mathbf{r}'$ where the value of $\mathbf{E}$ is different. That is, current and field are related non-locally by $\mathbf{j}(\mathbf{r}) = \int d\mathbf{r}' \sigma(\mathbf{r} - \mathbf{r}')\mathbf{E}(\mathbf{r}')$ where the non-local conductivity $\sigma(\mathbf{r})$ has range ℓ. Sharvin [9] found when $\ell/D \gg 1$ the smaller conductance $G_{\mathrm{S}} = 1/R_{\mathrm{S}} = G_{\mathrm{M}}(3\pi D/16\ell)$. Sharvin's answer can be written

$$G = G_0[A_c k_{\mathrm{F}}^2/4\pi] \quad \text{where} \quad G_0 = 2e^2/h \tag{9}$$

where A_c is the area of the constriction. The factor $2e^2/h = G_0 = 0.775 \times 10^{-4}\,\Omega^{-1}$ is the "quantum unit of conductance," while the second factor is the number of quantum "channels" that can carry current through the orifice. Consider for example a square orifice of side d. The spacing of k-states (e.g. $\sin(k_x x)\sin(k_y y)$) whose nodes are on the boundaries of the orifice is π/d in the directions x and y in the plane of the orifice. Counting the number of such states which are occupied and lie in the quarter circle $|(k_x, k_y)| < k_{\mathrm{F}}$ yields the second factor $[A_c k_{\mathrm{F}}^2/4\pi]$. The crossover between the Maxwell and Sharvin limits was studied by Wexler [10] and Nikolic and Allen [11]. They found the interpolation formula,

$$R = R_{\mathrm{S}} + \gamma(D/\ell)R_{\mathrm{M}} \tag{10}$$

where the numerical correction $\gamma(x)$ is fitted by the Padé approximation $\gamma = (1 + 0.83x)/(1 + 1.33x)$.

Sharvin's answer is only valid if the number of channels is large. When the dimensions of the channel become comparable to the Fermi wavelength, so that the number of channels is of order one, the size quantization of wavefunctions transverse to the channel results in the conductance G being quantized in approximate integer units of G_0. This effect, shown in Fig. 3, was first seen by van Wees et al. [12,13] and Wharam et al. [14], using devices made from a "two-dimensional electron gas" (2deg). Long mean-free paths are available near interfaces in GaAs/Al$_{1-x}$Ga$_x$As "quantum well" structures. Metallic gate electrodes deposited above the 2deg provide a way to tune the width of a constriction, known as a "quantum point contact."

There is a very simple argument which gives the quantized conductance $G = nG_0$, and which will be used as a starting point for the discussion of the Landauer formula in the next chapter. Let the gate potential at the gate axis $y = 0$ of Fig. 3 be modeled as $V(x, y = 0) = V_0 + m\omega_0^2 x^2/2$. Near the constriction, the wavefunctions in effective mass approximation are $\exp(ik_y y)H_n(x)\exp(-x^2/2x_0^2)$, that is, propagating in the y direction and harmonically confined in the x direction. The energy levels are $eV_0 + (c + 1/2)\hbar\omega + \hbar k_y^2/2m^*$. The integer $c \geqslant 0$ is the "channel index." Inset (b) of Fig. 3 shows the occupied levels for a gate voltage near -1.8 V, where three sub-bands in the constriction are partly occupied. The inset also indicates that a small source-drain bias has been applied, $\mu_L - \mu_R = -eV_{SD}$, where L and R refer to $y > 0$ and $y < 0$. The current through the constriction is caused by ballistic propagation. We just have to count the imbalance between left- and
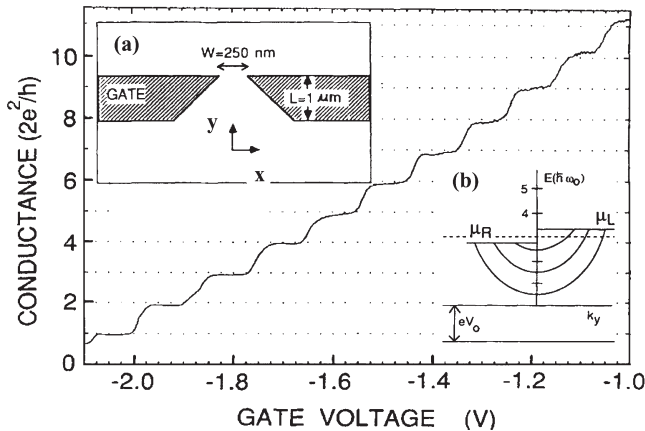

Fig. 3. Quantized conductance. The inset shows schematically the gate electrodes deposited in the insulating layer above a 2d electron gas (2deg, or GaAs quantum well). Varying the gate potential causes a variable width constriction for electrons of the 2deg. This device is called a "quantum point contact" (from van Wees et al. [12], [13]).

right-propagating states.

$$I = \frac{2}{L} \sum_c \sum_k (-ev_{kc})F(kc) \tag{11}$$

where the non-equilibrium occupancy is $F(kc) = f(\varepsilon_{kc} - \mu + \text{sign}(v_{kc})\Delta\mu/2)$ and $f(\varepsilon_{kc} - \mu)$ is the equilibrium Fermi–Dirac function of the state with longitudinal wavevector k and channel c. Left- and right-propagating states have Fermi levels shifted up and down by $\Delta\mu/2 = (\mu_L - \mu_R)/2$, and the factor of 2 is for spin degeneracy. For each channel, k is quantized in a fictitious box $-L/2 < k < L/2$ in the y direction with the orifice at the center. An occupied state transports charge $-e$ through the orifice in time L/v_{kc}. The box is long enough such that the spacing $\Delta k = 2\pi/L$ between k states is small. Convert the sum $\sum_k$ into an integral $(L/2\pi) \int dk$, and convert the integration step dk into $d\varepsilon_{kc}/\hbar v_{kc}$. The factors of velocity v_{kc} cancel, so each channel that intersects the Fermi level makes the same contribution. Thus we get

$$I = \frac{-2eN_c}{h} \int d\varepsilon [f_L - f_R] = G_0 N_c V_{SD} \tag{12}$$

where N_c is the number of channels intersecting the Fermi level. Each occupied propagating sub-band gives a current $G_0 V_{SD}$ which increases ohmically with $|\mu_L - \mu_R|$. At gate voltages less than -2.2 V, the upper ($y > 0$) and lower ($y < 0$) halves of the 2deg are decoupled, and G is essentially zero. At higher gate voltages, more and more sub-bands become partly occupied, and the conductance rises in steps of height $G_0 = 2e^2/h$ each time a new sub-band dips below the Fermi level.

One may ask, what is the source of resistance $1/G$ in this case where there is no evident source of dissipation? Note that the conductance does not depend on the longitudinal size L which is the total path length of current flow, so that the dissipated heat per unit volume goes to zero in the large size limit. The non-zero value of $1/G$ should be considered a "contact resistance" between the narrow "channel" and the macroscopic electrodes. De Picciotto et al. [15] have verified that a 4-terminal resistance measurement on a ballistic quantum wire gives an inherent resistance of zero, so the quantum resistance $1/N_C G_0$ is safely assigned to the contacts which were outside their voltage probes.

The details of coherent quantum flow in a ballistic quantum point contact were imaged by Topinka et al. [16], giving a most beautiful visual verification of the coherent electron states in the different channels.

The point contact turns out to be a useful probe, as Sharvin anticipated. In common with other junction devices, it permits a significant bias ΔV across a short channel, and thus a much larger **E**-field than can be achieved in a bulk conductor. Further, the small transverse dimension makes less stringent demands on microfabrication than does a larger area "planar" junction. Section 5 gives an example.

4. KUBO AND OTHER FORMULAS

In this chapter, some of the basic formulas [17] of transport theory are summarized and discussed.

4.1. Kubo Formulas

We consider an applied field $\mathbf{E} = -(1/c)\partial\mathbf{A}/\partial t$, with monochromatic frequency-dependence $\mathbf{E} = (i\omega/c)\mathbf{A}$. The current operator is

$$\hat{j}_{\text{tot},\alpha} = (ine^2/m\omega)E_\alpha + \hat{j}_\alpha,$$
$$\hat{j}_\alpha = -\frac{e}{m}\sum_i p_{i\alpha} \tag{13}$$

where $\mathbf{p}_i$ is the momentum operator for the ith electron. The first term of $\hat{j}_{\text{tot}}$ is the "diamagnetic" part related to the substitution $\mathbf{p}_i \to \mathbf{p}_i + e\mathbf{A}(\mathbf{r}_i, t)/c$. The Hamiltonian of the system is

$$H_{\text{tot}} = H + H_{\text{ext}},$$
$$H_{\text{ext}} = -\hat{\mathbf{j}} \cdot \mathbf{A}/c = (i/\omega)\hat{\mathbf{j}} \cdot \mathbf{E} \tag{14}$$

where the "unperturbed" part H contains all the equilibrium properties of the interacting system. We want to calculate the current $\text{tr}\hat{\rho}_{\text{tot}}\hat{j}_{\text{tot},\alpha}$ to first order in $\mathbf{E}$. The density matrix $\hat{\rho}_{\text{tot}}$ is perturbed away from its equilibrium value $\rho = \exp(-\beta H)/Z$ by the field, and we need to know the correction $\delta\hat{\rho}$ to first order in $\mathbf{E}$. First-order time-dependent perturbation theory for $\delta\hat{\rho}$ can be written in operator language using standard field-theoretic methods [18,19] as

$$\delta\hat{\rho}(t) = -\frac{i}{\hbar}e^{-iHt/\hbar}\int_{-\infty}^{t} dt'[H_{\text{ext}}(t'), \hat{\rho}]e^{iHt/\hbar} \tag{15}$$

where the time dependence of $H_{\text{ext}}(t')$ has two sources, first the fixed time dependence $\exp(-i\omega t')$ of the classical field $\mathbf{A}(t)$, and second, the Heisenberg time-dependence, $\hat{j}(t) = \exp(iHt/\hbar)\hat{j}\exp(-iHt/\hbar)$ assigned to operators. The frequency ω is assigned a small positive imaginary part $\omega \to \omega + i\eta$, which has the effect that at time $t = -\infty$, the perturbation vanishes and the density matrix has its equilibrium value. The Kubo formula [17–19] for the conductivity then follows by simple manipulation. It has at least two important versions,

$$\sigma_{\alpha\beta}(\omega) = \frac{ine^2}{m\omega}\delta_{\alpha\beta} + \frac{1}{\hbar\omega V}\int_0^\infty dt e^{i\omega t}\langle[\hat{j}_\alpha(t), \hat{j}_\beta(0)]\rangle \tag{16}$$

$$\sigma_{\alpha\beta}(\omega) = \frac{1}{V}\int_0^\beta d\lambda \int_0^\infty dt e^{i\omega t}\langle\hat{j}_\alpha(-i\hbar\lambda)\hat{j}_\beta(t)\rangle \tag{17}$$

The angular brackets $\langle\hat{Q}\rangle \equiv \text{tr}(\hat{\rho}\hat{Q})$ mean a canonical ensemble average using the equilibrium density matrix. The first version, Eq. (16), has the usual form [18] from

linear response theory of a "retarded" commutator correlation function. The word "retarded" refers to the fact that the commutator is set to zero for $t<0$, as is appropriate for a causal or retarded response. The first term of this expression, which comes from the diamagnetic part of the current operator, is singular, diverging as $\omega \to 0$. This divergence cancels against pieces from the second term.

The second version, Eq. (17) gets rid of the commutator and the singular first term, at the cost of introducing an imaginary time $-i\hbar\lambda$. This is treated like a real time, with the replacement $t \to -i\hbar\lambda$ in the Heisenberg time evolution. It can be derived from Eq. (16) using an operator identity for the density matrix,

$$[\hat{Q}, \hat{\rho}] = -i\hbar\hat{\rho} \int_0^\beta d\lambda \dot{\hat{Q}}(-i\hbar\lambda) \tag{18}$$

where the time derivative of $\hat{Q}$ is $(i/\hbar)[H, \hat{Q}]$.

To analyze these formulas, let us pretend that we know a complete set of many-body eigenstates $H|n\rangle = E_n|n\rangle$ of the system before the field is applied. Then we get from Eqs. (16) and (17) the "spectral representations"

$$\sigma_{\alpha\beta}(\omega) = \frac{ine^2}{m\omega}\delta_{\alpha\beta} + \frac{i}{\omega V}\sum_{mn}\frac{e^{-\beta E_n} - e^{-\beta E_m}}{Z}\frac{\langle n|j_\alpha|m\rangle\langle m|j_\beta|n\rangle}{\hbar(\omega + i\eta) - (E_m - E_n)} \tag{19}$$

$$\sigma_{\alpha\beta}(\omega) = \frac{i\hbar}{V}\sum_{mn}\frac{e^{-\beta E_n} - e^{-\beta E_m}}{Z(E_m - E_n)}\frac{\langle n|j_\beta|m\rangle\langle m|j_\alpha|n\rangle}{\hbar(\omega + i\eta) - (E_m - E_n)} \tag{20}$$

where the positive infinitesimal η has been added ($\omega \to \omega + i\eta$) to make the time integrals well defined. Because the denominators have imaginary parts which are delta functions, it is easy to show that both expressions have the same real part. This real part can be written in spectral representation, and then resummed as a correlation function,

$$\mathrm{Re}\,\sigma_{\alpha\beta}(\omega) = \frac{\pi}{\omega V}\sum_{mn}\frac{e^{-\beta E_n} - e^{-\beta E_m}}{Z}\langle n|j_\alpha|m\rangle\langle m|j_\beta|n\rangle\delta(\hbar\omega - (E_m - E_n)) \tag{21}$$

$$\mathrm{Re}\,\sigma_{\alpha\beta}(\omega) = \frac{1 - e^{-\beta\hbar\omega}}{2\hbar\omega V}\int_{-\infty}^{\infty} dt e^{i\omega t}\langle j_\alpha(t)j_\beta(0)\rangle \tag{22}$$

This last version of the Kubo formula is known as the "fluctuation-dissipation" theorem, because it relates the random current fluctuations of the equilibrium system $\langle j(t)j(0)\rangle$ to the dissipative part $\mathrm{Re}\,\sigma$ of the conductivity. The spectral version Eq. (21) is the same as the Fermi golden rule for the rate of absorption of energy by the system from the electromagnetic field *via* the perturbation $H_{\mathrm{ext}} = -\mathbf{j} \cdot \mathbf{A}/c$. The Kubo formulas Eqs. (16) and (17) are the results of lowest-order time-dependent perturbation theory in powers of the external field. This formula is the starting point for many-body perturbation theory using the response of a non-interacting system as a reference.

4.2. Kubo–Greenwood Formula

Often materials are successfully approximated as non-interacting Fermi systems. The Hamiltonian is the sum $\sum_i H_0(i)$ of identical single-particle Hamiltonians for each electron. The single-particle eigenstates $H_0|n\rangle = \varepsilon_n|n\rangle$ are a convenient basis, and the current operator can be written as

$$\hat{j}_x(t) = \sum_{nm} \langle n|j_x|m\rangle c_n^\dagger c_m e^{i(\varepsilon_n - \varepsilon_m)t/\hbar} \tag{23}$$

For an interacting system the same basis is used, and the same operator expression works at $t = 0$, but the Heisenberg time dependence of the current operator can no longer be written out explicitly. To evaluate the Kubo formulas, Eqs. (16) and (17), in non-interacting approximation Eq. (23), we need

$$\mathrm{tr}\hat{\rho}([c_n^\dagger c_m, c_p^\dagger c_q]) = \delta_{mp}\delta_{nq}(f_n - f_m)$$
$$\mathrm{tr}\hat{\rho}(c_n^\dagger c_m c_p^\dagger c_q) = \delta_{mp}\delta_{nq}f_n(1 - f_m) + \delta_{nm}\delta_{pq}f_n f_p \tag{24}$$

Here, $f_n = (\exp(\beta\varepsilon_n) + 1)^{-1}$ is the Fermi–Dirac occupation factor. Either procedure leads to

$$\sigma_{\alpha\beta}(\omega) = \frac{i\hbar}{V}\sum_{mn}\left(\frac{f_n - f_m}{\varepsilon_m - \varepsilon_n}\right)\frac{\langle n|j_\alpha|m\rangle\langle m|j_\beta|n\rangle}{\hbar(\omega + i\eta) + (\varepsilon_n - \varepsilon_m)} \tag{25}$$

To get this result from Eq. (19) requires separating denominators $1/\hbar\omega(\hbar\omega + \Delta)$ into $1/\Delta$ times $1/\Delta - 1/(\hbar\omega + \Delta)$ and then cancelling the first term against the diamagnetic part of Eq. (16) by use of operator relations $p_\alpha = (im/\hbar)[H, r_\alpha]$ and $[r_\alpha, p_\beta] = i\hbar\delta_{\alpha\beta}$.

First, let us interpret Eq. (25) for the case of a perfect crystal. The single particle quantum number n is now $(\mathbf{k}n\sigma)$, the current matrix elements are $\mathbf{k}$-diagonal, and the sum over n, m goes over transitions between filled and empty band states. For a semiconductor or insulator, this is the usual band-theoretic optical interband conductivity. For a metal, we have additional diagonal elements $\langle n|j_\alpha|n\rangle$ which equal $-ev_{\mathbf{k}n\alpha}$. The $n = m$ diagonal part of $(f_n - f_m)/(\varepsilon_m - \varepsilon_n)$ must be interpreted as $-\partial f(\varepsilon_{\mathbf{k}n})/\partial\varepsilon_{\mathbf{k}n}$. This can be understood by remembering that the electric field in an optical experiment is not strictly homogeneous but has a wavevector $\mathbf{q}$ with $q = \omega/c$ small on the scale of the Brillouin zone. The current matrix elements are then not diagonal, but defined between states of wavevector $\mathbf{k}$ and $\mathbf{k} + \mathbf{q}$. The limit $q \to 0$ goes smoothly. The resulting intraband piece of Eq. (25) is

$$\sigma_{\mathrm{intraband},\alpha\beta}(\omega) = \left(\frac{ie^2}{\omega + i\eta}\right)\left[\frac{1}{V}\sum_{\mathbf{k}n}\left(-\frac{\partial f}{\partial\varepsilon_{\mathbf{k}n}}\right)v_{\mathbf{k}n\alpha}v_{\mathbf{k}n\beta}\right] \tag{26}$$

This is exactly the Drude result, Eq. (6), except that the true collision rate $1/\tau$ is replaced by the infinitesimal η, reflecting the absence of collisions in the non-interacting perfect crystal. The factor in square brackets above is the Drude $(n/m)_{\mathrm{eff}}$, written correctly as a tensor which becomes a scalar for high-symmetry solids.

To really derive the Drude conductivity including collisions from the Kubo formula, the correct route is through a Boltzmann equation. There are convincing derivations of the linearized Boltzmann equation starting from the Kubo formula [20–22]. The derivations are quite tedious. Amazingly, the correct (and not linearized) Boltzmann equation was guessed by Bloch long before the advanced perturbative techniques were available. The reasons for Bloch's success were clarified by Landau. Solving the Bloch–Boltzmann equation in all generality is also not easy. Simple approximations work well much of the time, and allow an easy alternate derivation of the Drude $(n/m)_{\mathrm{eff}}$. This will be shown in Section 6.2, especially Eq. (55) which gives further interpretation.

The Boltzmann approach works only if the crystal is pure enough, and has weak enough interactions, that the wavevector $\mathbf{k}$ is a fairly good quantum number. This fails in dirty alloys, yet a single-particle approximation may still be good. Therefore, Eq. (25) has a range application outside of Boltzmann theory. This is discussed in Section 8. Eq. (25) is often rewritten in terms of the single-particle Green's function

$$\hat{G}^+(E) = \frac{1}{E + \mathrm{i}\eta - \hat{H}_0} \quad \hat{G}^-(E) = \frac{1}{E - \mathrm{i}\eta - \hat{H}_0}$$

$$\hat{G}^{\times}(E) = \frac{1}{2\pi i}(\hat{G}^+ - \hat{G}^-) = \sum_n |n\rangle \delta(E - \varepsilon_n)\langle n|$$

$$\hat{G}^{\times}(x, x', E) = \langle x|\hat{G}^{\times}(E)|x'\rangle = \sum_n \psi_n(x)\psi_n^*(x')\delta(E - \varepsilon_n) \tag{27}$$

The notation is that of Ziman [23]. The label x denotes $(\mathbf{r}\sigma)$, the space and spin coordinates of the electron. The non-interacting Kubo formula in the dc limit can be written as

$$\sigma_{\alpha\beta} = \frac{\pi e^2 \hbar}{m^2 V} \int \mathrm{d}x\, \mathrm{d}x' \left(\frac{\hbar}{i}\nabla_\alpha G^{\times}(x, x', \varepsilon_{\mathrm{F}})\right)\left(\frac{\hbar}{i}\nabla'_\beta G^{\times}(x', x, \varepsilon_{\mathrm{F}})\right) \tag{28}$$

where $\nabla_\alpha = \partial/\partial r_\alpha$ and $\nabla'_\beta = \partial/\partial r'_\beta$. This is called the "Kubo–Greenwood" formula [17,24]. It is not any different from the previous version Eq. (25), but is useful if the disorder is treated perturbatively. One then averages over an ensemble of different representatives of the disorder. The correct procedure is to average the product of the two Green's functions. This is not the same as multiplying two separately averaged Green's functions. The latter procedure, for example, does not permit Anderson-insulating behavior in very disordered electron systems. The reason is that the averaged G loses off-diagonal information and cannot distinguish localized from delocalized states.

4.3. Conductance as Transmission

When coherent electron transmission plays a role, Kubo and Boltzmann formulations become less appropriate than an analysis starting from scattering theory [25–29]. Consider the system shown schematically in Fig. 4. On the left and right are
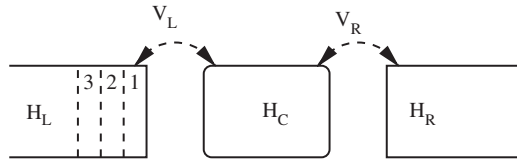
Fig. 4. Schematic diagram of a system with two ideal leads on left and right, modeled as semi-infinite and described by Hamiltonians H_L and H_R. In the center is an island which is coupled to the leads (perhaps weakly or perhaps strongly) by coupling matrix elements V_L and V_R. The material in the center (described by H_C) can be an oxide barrier, vacuum, a disordered metal, or a molecule.

perfect metals regarded as electrodes. The central section may have disorder, or an oxide barrier, or a vacuum break (modeling a scanning tunneling microscope, for example), or perhaps a break which has been filled with some molecular bridge material. The left and right ballistic leads each have their own chemical potential, μ_L and μ_R, set by distant reservoirs which are not modeled explicitly. Choosing each electrode sequentially as a source of incident waves, the Schrödinger equation is solved for the amplitude of transmission into the other electrode (or electrodes in a multi-terminal device). We may not wish to average over an ensemble of related systems, but instead might wish to study the interesting idiosycracies of some particular system.

The scattering state wavefunction for a state incident from the left is

$$|\psi_{knL}\rangle = |knL\rangle + \sum_m r(k)_{mn}|-kmL\rangle \quad \text{on the left}$$

$$= \sum_m t(k)_{nm}|kmR\rangle \quad \text{on the right} \qquad (29)$$

where r and t are reflection and transmission coefficients connecting the incident state $|knL\rangle$ to reflected $|-kmL\rangle$ and transmitted $|kmR\rangle$. Here k is the 1D wave-vector for propagation along the electrode; it is not necessarily the same on left (L) and right (R). Each electrode has possibly many "channels" or tranverse quantum states n, m near the Fermi level. At fixed energy each channel has a different k. When left and right electrodes are inequivalent, the states $|knL, R\rangle$ are normalized with a factor of $\sqrt{(v_{knL,R})}$ so that unitary transmission matrices t_{mn} are required by current conservation. The conductance of this system was already discussed in Section 3 for the ballistic case $t = \delta_{mn}$ and $r = 0$. When there is non-zero scattering, Eq. (12) generalizes to [25,26]. This is a Landauer formula [25,29]. In the Ohmic limit $I = GV$ we get

$$I = \frac{2e}{h} \int d\varepsilon [f_L(\varepsilon) - f_R(\varepsilon)] \text{tr}[t^\dagger t(\varepsilon)] \qquad (30)$$

$$G = G_0 \text{tr}(t^\dagger t) \qquad (31)$$

The 2 is for spin, and the Fermi–Dirac functions $f_{L,R}(\varepsilon)$ are $(\exp(\beta(\varepsilon - \mu_{L,R}) + 1)^{-1}$. Equation (31) follows from (30) in the limit where the source-drain bias

$V_{SD} = (\mu_L - \mu_R)/e$ is smaller than the characteristic energies of the leads or of the system between the leads. Equation (30) goes beyond the Kubo approach in allowing bias voltages outside the regime of linear response. However, inelastic scattering effects do not easily get incorporated.

There is a more general approach using non-equilibrium Green's function (NEGF) theory, discussed by Meir and Wingreen [30,31], which in principle permits a full treatment of interactions and inelastic scattering, but is not easy to implement. In the non-interacting limit, a result is found equivalent to Eq. (30), but more convenient for computation. The derivation was first given by Caroli et al. [31]. The total Hamiltonian is written

$$H_{tot} = H_L + [V_L + H_C + V_R] + H_R \qquad (32)$$

Whereas the scattering method treats the three terms in square brackets as one scattering potential, now we think separately of the solutions to the three pieces described by H_L, H_R, and H_C. Long-range interactions between different subsystems are omitted. The parts of the Hamiltonian are usually expressed in a basis of single-particle local orbitals. The single-particle Schrödinger equation in schematic form is

$$\begin{pmatrix} H_L - \varepsilon & V_L & 0 \\ V_L^\dagger & H_C - \varepsilon & V_R \\ 0 & V_R^\dagger & H_R - \varepsilon \end{pmatrix} \begin{pmatrix} \psi_L \\ \psi_C \\ \psi_R \end{pmatrix} = 0 \qquad (33)$$

Let us suppose that we can find the separate "partial" Green's functions

$$g_L(\varepsilon) = (\varepsilon - H_L)^{-1}$$
$$g_C(\varepsilon) = (\varepsilon - H_C)^{-1}$$
$$g_R(\varepsilon) = (\varepsilon - H_R)^{-1} \qquad (34)$$

For the central region, perhaps the system is small enough that we can solve $H_C|C\rangle = E_C|C\rangle$ exactly by some method. The L and R electrodes are semi-infinite, and almost periodic except that the termination at the central region destroys translational invariance. We prefer not to find explicit solutions $H_L|L\rangle = E_L|L\rangle$ and $H_R|R\rangle = E_R|R\rangle$. It turns out that the partial Green's function $g_L(x, x')$ is only needed for x, x' lying in the surface region labeled 1 on Fig. 4, and similarly for g_R. If the surface part 1 couples by V_{12} to layer 2, and is decoupled from other interior layers, and if identical matrices V_{23}, etc. couple the other layers, then there is a closed equation which can be solved iteratively, with $g_L^{(n)}$ approaching g as $n \to \infty$, namely

$$g_L^{(n+1)} = (\varepsilon - h_1 - V_{12}^\dagger g_L^{(n)} V_{12})^{-1} \qquad (35)$$

where h_1 is the part of H_L confined to layer 1, assumed identical in form to h_2, etc. There is an alternate method to calculate g_L due to Kalkstein and Soven [32]. Therefore all three partial Green's functions may be calculable. They can be used to

find the transmission and the current

$$I = \frac{4\pi e}{\hbar} \int_{-\infty}^{\infty} d\varepsilon \sum_{LR} |\langle L|\hat{T}|R\rangle|^2 \delta(\varepsilon - E_L)\delta(\varepsilon - E_R)[f_L(\varepsilon) - f_R(\varepsilon)] \tag{36}$$

without explicitly finding $|L\rangle$, or E_L, etc. The transmission matrix $\hat{T}$ is given by the Lippman–Schwinger equation,

$$\hat{T} = (V_L + V_R) + (V_L + V_R)^\dagger G(\varepsilon)(V_L + V_R) \tag{37}$$

where $G = (\varepsilon - H)^{-1}$ is the Green's function of the whole system. We assume the central region large enough that there are no direct couplings, $0 = \langle L|V_L + V_R|R\rangle$. Therefore the off-diagonal parts of the $\hat{T}$ matrix are

$$\langle L|\hat{T}|R\rangle = \sum_{MM'} \langle L|V_L^\dagger|M\rangle\langle M|G|M'\rangle\langle M'|V_R|R\rangle \tag{38}$$

From this we see that the system's Green's function matrix $G(x, x')$ is only needed for x, x' in the central region where the eigenstates are $|M\rangle, |M'\rangle$. Denoting this submatrix as G_C, and doing some matrix algebra, we find

$$G_C(\varepsilon) = (\varepsilon - H_C - \Sigma_L - \Sigma_R)^{-1} \tag{39}$$

where the self-energies $\Sigma_{L,R}$ contain the shift and broadening of the states of the central region which come from coupling to the leads,

$$\Sigma_L(\varepsilon) = V_L^\dagger g_L(\varepsilon) V_L \quad \Sigma_R(\varepsilon) = V_R^\dagger g_R(\varepsilon) V_R \tag{40}$$

Now we are ready to rewrite Eq. (36) in terms of this central part of the Green's function. The self-energies $\Sigma_{L,R}$ have imaginary parts

$$\langle N|\Gamma_L|M\rangle = -2\text{Im}\langle N|\Sigma_L(\varepsilon + i\eta)|M\rangle$$
$$= 2\pi \sum_L \delta(\varepsilon - E_L)\langle N|V_L|L\rangle\langle L|V_L^\dagger|M\rangle \tag{41}$$

and similarly for Γ_R. Now we can express the current as

$$I = \frac{2e}{h} \int_{-\infty}^{\infty} d\varepsilon\, \text{tr}[\Gamma_L G_C(\varepsilon - i\eta)\Gamma_R G_C(\varepsilon + i\eta)][f_L(\varepsilon) - f_R(\varepsilon)] \tag{42}$$

where the trace goes over states of the central region only.

This equation is widely used to calculate the conductance dI/dV_{SD} both in the linear regime of small source-drain bias and beyond the linear regime, for small molecules or other small systems. For example, "exact" single-particle eigenstates of a model dirty alloy may be found for small samples, of order 100 atoms. Calculation of resistivity by direct application of the Kubo–Greenwood formula has some difficulties because of the discreteness of the spectrum. These difficulties are nicely smoothed over if the small system is attached to two ideal leads and Eq. (42) is used [33–35]. For molecular applications, theory and experiment for the non-linear $G(V)$ curves do not often agree closely. The subject is under rapid development [36–40].

5. SUPERCURRENT AND ANDREEV REFLECTION

Supercurrent j_S is a collective motion of the superconducting condensate, Eq. (2). The order parameter ψ is related to the pair amplitude $\langle c_{k\uparrow} c_{-k\downarrow} \rangle$, which gives the occupancy of a Cooper pair state built from the time-reversed pair of electrons $(k \uparrow, -k \downarrow)$. The pair amplitude acquires a current-carrying phase factor $\exp(i\mathbf{q} \cdot \mathbf{r})$ if all states $k' \uparrow$ and $-k' \downarrow$ are shifted by $\mathbf{q}/2$. Then the current is $\mathbf{j}_S = -2en_S\hbar\mathbf{q}/m$.

Andreev [41] explained how a current in a normal metal (N) can flow across the N/S boundary to the superconducting (S) side. An incident N quasiparticle $k \uparrow$ with current $-e\mathbf{v}_k$ can convert directly (with some amplitude for reflection as well as transmission) into a current-carrying S excited quasiparticle, but only if the N energy $\varepsilon_k - \mu$ exceeds the S gap Δ. If $|\varepsilon_k - \mu| < \Delta$, this is not possible, and the only route is for the incident N electron to bind to another N electron $-k \downarrow$, entering the S side as a Cooper pair. After this event, the N side lacks the $-k \downarrow$ electron, which means it has a hole with charge $+|e|$ and velocity $\mathbf{v}_{-k} = -\mathbf{v}_k$. This hole continues to carry N current $-e\mathbf{v}_k$, the same as the N current before the $k \uparrow$ state entered S. This process, called "Andreev reflection," doubles the current.

An elegant illustration [42] is shown in Fig. 5. A superconducting Nb wire was sharpened to make a point contact and carefully contacted to various clean normal metal surfaces (paramagnetic Cu and various ferromagnets). The conditions are not always reproducible, and only selected data were used for analysis. The selected
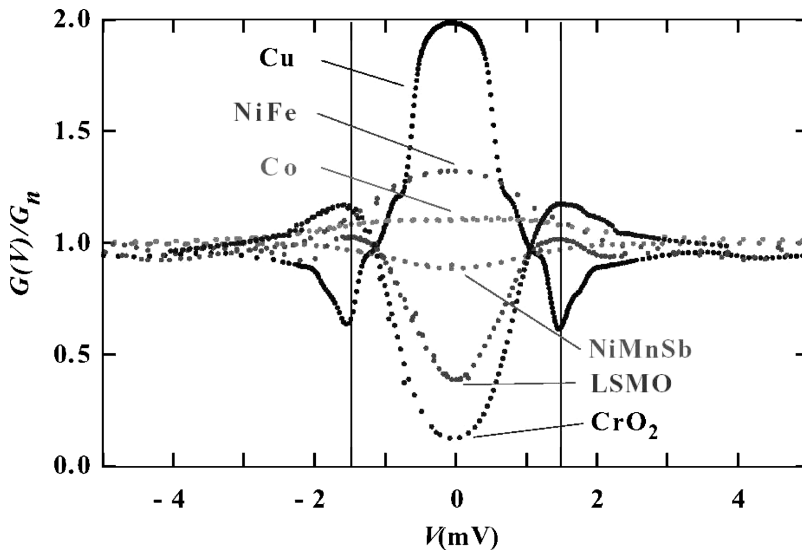

Fig. 5. Differential conductance dI/dV versus source-drain bias in a superconductor/normal point contact [42]. A superconducting Nb point is contacted to various metals. Cu shows the effect of Andreev reflection doubling the conductance at low bias, whereas the ferromagnetic samples with reduced minority spin population show suppression of the Andreev process.

data are believed to satisfy the criteria for Andreev reflection, cleanliness and transparency of the point contact. When the bias voltage V across the point contact is $\pm\Delta/e$ (the gap Δ of Nb is 1.5 meV, slightly higher than $3.52 k_B T_c/2$), structure is seen in the differential conductance $G = dI/dV$, arising from the BCS peak $1/\sqrt{E^2 - \Delta^2}$ in the quasiparticle density of states. At larger biases, $V > 2\Delta/e$, G is independent of bias and approaches the conductance of the normal metal N. At low biases, $|V| < \Delta/2e$, the conductance doubles in the Cu point contact as expected from Andreev reflection [43]. But CrO_2 is different in that there are no down-spin electrons near the Fermi level. It is a "half-metallic" ferromagnet, meaning that the minority spins have an insulating gap while the majority spins are metallic. Therefore, in CrO_2, no Andreev process is possible, and the conductance is essentially zero at small bias. Other ferromagnets, which have reduced but non-zero numbers of minority carriers at the Fermi level, show an intermediate effect. Analysis using the theory of Blonder et al. [43] indicates a point contact area $\approx 10^4 \overset{\circ}{A}^2$, large compared to the area $< 100 \overset{\circ}{A}^2$ where quantized conductance is expected as in Fig. 3.

This experiment illustrates an important theme of present-day nanoscale physics. Use of nanoscale devices can enormously enhance the view of phenomena which are also present in bulk but hard to access experimentally. The cost is that data may have to be selectively sorted based on theoretically inspired criteria, since control over fabrication is so primitive. This enlarges the opportunity for ill-considered claims (not illustrated here!) or outright fraud [44].

6. BLOCH–BOLTZMANN THEORY

Transport theory of solids began with Bloch's [4] thesis of 1928 which explained metallic resistivity. Landau [5] clarified the meaning of Bloch's work. Around 1962 theoretical tools improved to the point that the rigorous basis for Bloch's ideas became clear [20–22]. Since around 1980 [45,46] it has been possible to compute with Bloch's theory for metals with non-trivial band structures, which fully tests the theory. It has also been possible to go outside the validity of Bloch's theory to calculate the resistivity of dirty alloys, liquid metals, and amorphous metals, using one-electron theory and neglecting inelastic scattering.

Following Landau [5], assume that there exist single-particle-like electron excitations, and that the occupation function or distribution function $F(k, \mathbf{r}, t)$ exists. F is an ensemble average non-equilibrium distribution. For large samples with homogeneous fields, the volume average equals the ensemble average, or the system is self-averaging. In small samples at low T, interesting deviations from self-averaging can be seen, requiring a more complete theory. Two effects cause F to evolve with t. First, scattering causes discontinuous changes of the quantum number k at some statistical rate. Second, there is smooth evolution arising from drift and acceleration of quasiparticles. Ignoring collisions, at a later time $t + \Delta t$, the new distribution $F(k, \mathbf{r}, t + \Delta t)$ will be the old distribution $F(k - \dot{k}\Delta t, \mathbf{r} - \dot{\mathbf{r}}\Delta t, t)$. This is expressed by

the Boltzmann equation

$$\frac{\partial F}{\partial t} + \dot{\mathbf{k}} \cdot \frac{\partial F}{\partial \mathbf{k}} + \dot{\mathbf{r}} \cdot \frac{\partial F}{\partial \mathbf{r}} = \frac{\partial F}{\partial t}\bigg|_{\text{coll}} \tag{43}$$

The left-hand side is the "co-moving" time derivative and the right-hand side takes account of collisions. Bloch [4] identified $\dot{\mathbf{r}}$ with $\mathbf{v}_k$ and $\hbar\dot{\mathbf{k}}$ with the force $-e(\mathbf{E} + \mathbf{v}_k \times \mathbf{B}/c)$ of applied fields. The collision term $(\partial F/\partial t)_{\text{coll}}$ was constructed using the probabilistic rules of t-dependent perturbation theory, and requires knowing the occupancies $F(k')$ of all other states k'. The theory is amazingly powerful and surprisingly accurate for a wide class of materials. It rests on assumptions of wide validity, although their truth is far from evident. The most fundamental underlying assumption was explained by Landau [5] – the assumption of the existence of "quasiparticles." A quasiparticle is an approximate excited state with charge $\pm|e|$, spin $\pm 1/2$, and a reasonably sharp wavevector $k \pm 1/\ell_k$ and energy $\varepsilon_k \pm \hbar/\tau_k$, where $\ell_k = v_k\tau_k$ is the mean free path and τ_k the time interval before the excitation loses its sharp definition in energy or momentum. In Section 6.6, the issue is discussed of whether band theory gives correct quasiparticle energies.

6.1. Technical Definition of Quasiparticle

The "temperature Green's function" $G(k,\sigma) = -\langle \hat{T} c_k(\sigma) c_k^\dagger(0) \rangle$ is the convenient object for perturbation theory. An imaginary time $it \to \sigma$ labels the electron destruction operators $c_k(\sigma) = \exp(\sigma H) c_k \exp(-\sigma H)$ and is ordered by the Wick operator $\hat{T}$. This Green's function is Fourier transformed into the imaginary Matsubara frequency $i\omega_v$, giving $G(k, i\omega_v)$. It is then analytically continued to the real frequency axis to give the retarded Green's function

$$G(k,\omega) = [\omega - \varepsilon_k - \Sigma(k, \omega + i\eta)]^{-1} \tag{44}$$

where $\Sigma(k, \omega + i\eta)$ is the complex self-energy which can be evaluated perturbatively. The imaginary part of G is the electron spectral function $A(k,\omega)$

$$A(k,\omega) = -\frac{1}{\pi} \text{Im} G(k,\omega) \tag{45}$$

For fixed k, the ω-dependence of $A(k,\omega)$ is interpreted as the spectrum of excitation energy that results from insertion of an electron into the system in state k outside the Fermi surface, or from insertion of a hole into the system in a state k inside the Fermi surface. The latter process is experimentally accessed in a photoemission experiment, and the former in an "inverse" photoemission experiment, although there are complicating details that weaken these interpretations [47,48]. If the Green's function has a simple pole $1/(\omega - \omega_k)$ at complex frequency ω_k, below the real ω axis by an amount $-\text{Im}\omega_k$, then $A(k,\omega)$ has a Lorentzian peak whose center defines the quasiparticle energy ε_k^* and whose width gives the relaxation rate $1/\tau_k^*$. We assume that the real part of the self-energy can be expanded for small ω as

$$\text{Re}\Sigma(k, \omega + i\eta) = \delta\varepsilon_k - \omega\lambda_k \tag{46}$$

Then we define

$$\varepsilon_k^* = \frac{\varepsilon_k + \delta\varepsilon_k}{(1 + \lambda_k)}$$

$$\frac{1}{\tau_k^*} = \frac{-2}{(1 + \lambda_k)} \operatorname{Im}\Sigma(k, \varepsilon_k^* + i\eta) \tag{47}$$

so that the spectral function has approximately the form of a Lorentzian lineshape,

$$A(k, \omega) = \frac{z_k}{\pi} \frac{\hbar/2\tau_k^*}{(\omega - \varepsilon_k^*)^2 + (\hbar/2\tau_k^*)^2} \tag{48}$$

Here $z_k = 1/(1 + \lambda_k)$ is called the wavefunction renormalization.

If $\hbar/\tau_k^*$ is small compared to relevant energies like $|\varepsilon_k^* - \mu|$, then the Lorentzian is sharp as a function of ω. We may identify ε_k^* as the "quasiparticle energy." However, the quasiparticle is only well defined if the spectral function is sharply peaked also as a function of $|\mathbf{k}|$. Expanding ε_k^* as $\varepsilon_F + \hbar \mathbf{v}_k^* \cdot (\mathbf{k} - \mathbf{k}_F)$, we must also require that $\ell_k^* = |\mathbf{v}_k^*|\tau_k^*$ be large enough compared to relevant distances $1/k_F$ or the lattice constant a.

This is actually not the only way to make a connection between G and a quasiparticle. When deriving a Boltzmann equation from the non-equilibrium version of G [21] it is preferable to define F by integration of G over the component $k_\perp$ of the k-vector perpendicular to the Fermi surface. This permits a Boltzmann equation to persist even for certain cases where the quasiparticle defined above fails to be narrow enough to recognize.

6.2. Solution for Conductivity

Consider a bulk material with a homogeneous dc electric field. A steady-state current flows, derivable using Eq. (1) from a steady-state non-equilibrium distribution $F(k) = f(k) + \delta F(k)$, where $f(k)$ is the Fermi–Dirac distribution $1/[\exp(\varepsilon_k/k_B T) + 1]^{-1}$. To find δF to first order in $\mathbf{E}$ it is necessary to solve the linearized equation of motion for F, that is, the linearized version of Eq. (43),

$$-e\mathbf{E} \cdot \mathbf{v}_k \frac{\partial f}{\partial \varepsilon_k} = -\sum_{k'} I(k, k')\delta F(k'). \tag{49}$$

The left-hand side is the linearized version of $\dot{\mathbf{k}} \cdot \partial F/\partial k$, and the right-hand side is the linearized collision integral. After suitable manipulations (explained in Refs. [49,50]) an integral equation with a Hermitean non-negative kernel is obtained. The non-negativity is required by the second law of thermodynamics and guarantees that entropy (which can be defined [51] for near-equilibrium Fermi gases by $S/k_B = -\sum[F_k \ln F_k + (1 - F_k)\ln(1 - F_k)]$) increases steadily in time until equilibrium is reached. The Hermitean operator can be inverted by brute force in k-space [45] or using smaller matrices after expansion in a convenient set of orthogonal polynomials [52,53]. The solution can be guided by a variational principle

(maximum entropy production) [49,50]. A general form of a variational *ansatz* is

$$F(k) = f(\mathbf{k} + e\mathbf{E}\tau_k/\hbar) \to f(k) + e\tau_k \mathbf{E} \cdot \mathbf{v}_k \left(\frac{\partial f}{\partial \varepsilon_k} \right) \qquad (50)$$

which represents a Fermi–Dirac distribution pulled off-center by the E-field. The displacement of the Fermi surface is governed by the k-dependent parameter τ_k which is varied to optimize the solution of the exact linearized equation. One can pretend that this "trial" solution follows from a "relaxation-time" representation of the Boltzmann equation,

$$\left(\frac{\partial F}{\partial t} \right)_{\text{coll}} \to -\sum_{k'} I(k,k') \delta F(k') \to -\frac{\delta F(k)}{\tau_k} \qquad (51)$$

However, the last form of this equation is *not* the true evolution equation. The τ_k which gives the exact solution of the real equation has no closed-form expression, and is definitely different from the quasiparticle lifetime τ_k^* defined above. One difference is that the "renormalization factor" $1 + \lambda_k$ in Eq. (47) is missing; all such factors cancel in the dc limit. Another difference is that a correction like $1 - \cos\theta_{kk'}$ needs to be included in the τ_k which solves the Boltzmann equation with a driving field. This factor suppresses the contribution of small angle scattering, because small angles do not much degrade the electrical current.

The formula for dc electrical conductivity is found from Eqs. (1) and (50)

$$\sigma_{xx} = \frac{e^2}{V} \sum_k v_{kx}^2 \tau_k \left(-\frac{\partial f}{\partial \varepsilon_k} \right) \qquad (52)$$

where τ_k depends on the details of the scattering and on the temperature, and remains to be determined. There is one standard variational trial solution which works quite well and gives convenient closed-form answers. If we assume that the parameter τ_k in Eq. (50) is τ_{tr}, independent of k, the Boltzmann equation will specify the optimal value of τ_{tr} which gives σ closest to the exact solution. The answer is

$$1/\tau_{\text{tr}} = \frac{\sum_{k,k'} v_{kx} v_{k'x} I_{k,k'} (-\partial f / \partial \varepsilon_k')}{\sum_k v_{kx}^2 (-\partial f / \partial \varepsilon_k)} \qquad (53)$$

Within this variational approximation we now have a closed-form approximation for the electrical conductivity,

$$\sigma = \left(\frac{n}{m} \right)_{\text{eff}} e^2 \tau_{\text{tr}} \qquad (54)$$

where τ is given by Eq. (53), and $(n/m)_{\text{eff}}$ is given by

$$\left(\frac{n}{m} \right)_{\text{eff}} = \frac{1}{V} \sum_k v_{kx}^2 \left(-\frac{\partial f}{\partial \varepsilon_k} \right) = \frac{1}{V} \sum_k \left(\frac{\partial^2 \varepsilon_k}{\partial (\hbar k_x)^2} \right) f_k \qquad (55)$$

The first version of Eq. (55) is convenient for numerical computation from band theory [54]. It was already derived by a different method in Eq. (26). Using the replacement $\delta(\varepsilon_k) = -\partial f / \partial \varepsilon_k$, the k-sum is restricted to the Fermi surface. The second

version is obtained from the first after integration by parts. In the second form, it is clear that $(n/m)_{\text{eff}}$ is the sum over occupied states of the reciprocal band effective mass. The sum over a filled band has positive and negative contributions and gives zero.

6.3. Orders of Magnitude

A big part of transport theory concerns [55] the phenomenological relaxation rate $1/\tau$. Let us estimate the order of magnitude of various contributions. There are three interactions (impurities, electron–phonon interactions, and Coulomb scattering) which always affect the lifetime of quasiparticles in metals,

$$H_{\text{imp}} = \sum_{kk'} V_{\text{imp}}(kk') S_{\text{imp}}(k - k') c_{k'}^{\dagger} c_k \tag{56}$$

$$H_{\text{ep}} = \sum_{kk'Q} V_{\text{ep}}(kk'Q) c_{k'}^{\dagger} c_k (a_Q^{\dagger} + a_{-Q}) \tag{57}$$

$$H_{\text{C}} = \sum_{1234} V_{\text{C}}(1234) c_1^{\dagger} c_2^{\dagger} c_3 c_4 \tag{58}$$

For magnetic materials, spin waves [56] and spin disorder also scatter. Here $S_{\text{imp}}(q)$ is the "impurity structure factor" $S_{\text{imp}} = \sum_i \exp(i\mathbf{q} \cdot \mathbf{R}_i)$ where $\mathbf{R}_i$ is the position of the ith impurity. The operator a_Q destroys the phonon of wavevector Q and energy ω_Q. Discrete translation symmetry gives a crystal momentum selection rule requiring the matrix element $V_{\text{ep}}(kk'Q)$ to vanish unless $\mathbf{k}' - \mathbf{k} = \mathbf{Q} + \mathbf{G}$ where $\mathbf{G}$ is a reciprocal lattice vector. The shorthand $(12\ldots)$ means $(k_1, k_2, \ldots)$, and crystal momentum conservation requires that $V_{\text{C}}(1234)$ vanishes unless $(\mathbf{k}_1 + \mathbf{k}_2 - \mathbf{k}_3 - \mathbf{k}_4)$ equals a reciprocal lattice vector.

One estimates the lifetimes from the Golden rule as follows:

$$\hbar/\tau_{\text{imp}} = 2\pi n_{\text{imp}} |V_{\text{imp}}|^2 N(0) \tag{59}$$

$$\hbar/\tau_{\text{ep}} = 2\pi n_{\text{ph}} |V_{\text{ep}}|^2 N(0) \tag{60}$$

$$\hbar/\tau_{\text{C}} = 2\pi n_{\text{pairs}} |V_{\text{C}}|^2 N(0) \tag{61}$$

where $N(0)$ is the density of states at the Fermi level. Here n_{imp} comes from averaging the impurity structure factor $\langle S(q_1) S(q_2) \rangle = n_{\text{imp}} \delta(q_1 + q_2)$. The factor n_{ph} is the number of phonons $\langle a^{\dagger} a \rangle$ which at high temperature is $k_B T / \hbar \omega_{\text{ph}}$. The factor n_{pairs} is the number of electron-hole pair states $(k_B T / \varepsilon_F)^2$ available for an electron to create when it scatters by the Coulomb interaction. Thus the orders of magnitude can be written

$$\hbar/\tau_{\text{imp}} \sim n_{\text{imp}} \varepsilon_F \tag{62}$$

$$\hbar/\tau_{\text{ep}} \sim k_B T \tag{63}$$

$$\hbar/\tau_{\text{C}} \sim (k_B T)^2 / \varepsilon_F \tag{64}$$

Here we use the fact that the typical impurity or Coulomb scattering matrix element is a few eV in magnitude, similar to the Fermi energy ε_F, while the electron–phonon matrix element $V_{ep} \sim \sqrt{(\hbar\omega_{ph}\varepsilon_F)}$ is smaller. Impurity scattering has $\hbar/\tau$ smaller than ε_F by the small parameter n_{imp}, electron–phonon scattering by the small parameter $(k_B T/\varepsilon_F)$, and Coulomb scattering by two factors of the same. At low T, impurity scattering always dominates (unless superconductivity intervenes and destroys the Fermi liquid). At high enough T, in principle, Coulomb scattering should dominate, but usually the required temperature is above the melting temperature. At intermediate temperatures, phonons dominate. At lower temperatures, the number of phonons decreases as the third rather than first power of $(k_B T/\hbar\omega_{ph})$, so there is a window at low T where the Coulomb interaction is larger than the electron–phonon interaction. Except for extremely clean metals, impurity scattering dominates Coulomb scattering in this window.

6.4. Computation of Resistivity

At the level of the variational solution Eqs. (53) and (54), the resistivity obeys Matthiessen's rule, being composed of additive parts from the various scattering mechanisms

$$1/\tau_{tr} = 1/\tau_{imp} + 1/\tau_{ep} + 1/\tau_{ee} \tag{65}$$

The dominant source of deviation from Mattheisson's rule is not because of higher than second-order effects where different scattering mechanisms mix, but rather in the fact that the true solution for the displacement τ_k of the Fermi distribution can reoptimize if the different scattering processes have differing anisotropies. The fact that measured deviations from Matthiessen's rule [57] are small indicates that the lowest order variational solution is generally quite good. Successful computation [58] of deviations from Matthiessen's rule shows that Bloch–Boltzmann theory is correct in many details.

Using general properties of the linearized collision integral $I(k, k')$, it has been shown [49,50] that the variational formula Eq. (53) can be written as

$$1/\tau_{tr} = \frac{\sum_{kk'}(v_{kx} - v_{k'x})^2 P_{kk'}}{2k_B T \sum_k v_{kx}^2(-\partial f/\partial\varepsilon_k)} \tag{66}$$

where $P_{kk'}$ is the rate of transitions from state k to state k' for the system in equilibrium. This is non-negative, and symmetric ($P_{kk'} = P_{k'k}$) which is the "principle of detailed balance." The factor $(v_{kx} - v_{k'x})^2$ becomes $(2v_F^2/3)(1 - \cos\theta_{kk'})$ in spherical symmetry.

Using the Hamiltonian Eq. (57), and writing $V_{ep}(kk'Q)$ as $M(kk')\delta(k' - k - Q)$, it is convenient to define a class of "electron–phonon spectral functions"

$$\alpha_w^2 F(\Omega) = N(0)\frac{\sum_{kk'}|M(kk')|^2 w(k, k')\delta(\Omega - \omega_{k-k'})\delta(\varepsilon_k)\delta(\varepsilon_{k'})}{\sum_{kk'} w(k, k')\delta(\varepsilon_k)\delta(\varepsilon_{k'})} \tag{67}$$
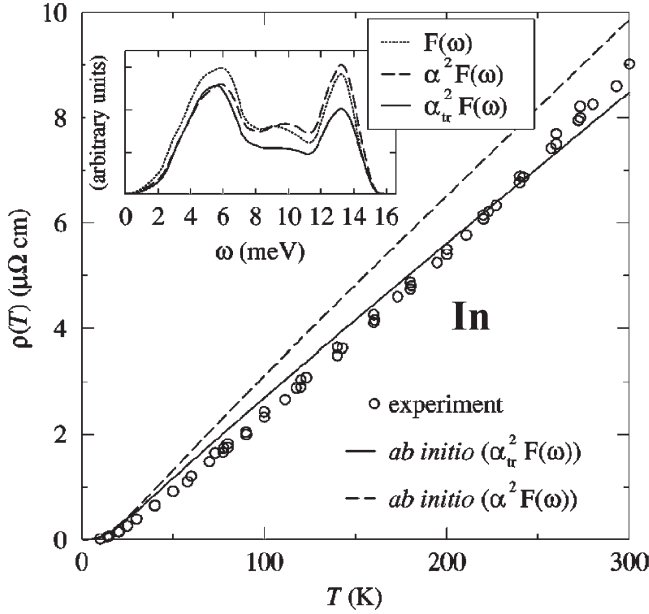
Fig. 6. Calculated resistivity of In versus T [63]. The two theoretical curves are computed using the spectral functions shown in the inset. The dashed line uses $\alpha^2 F$ (corresponding coupling constant $\lambda = 0.88$), and the solid line uses $\alpha_{tr}^2 F$ (coupling constant $\lambda_{tr} = 0.74$. The inset shows the similarity of these functions to the empirical phonon density of states.

The weight function $w(k, k')$ has various forms. When $w = 1$, the function called $\alpha^2 F$ appears in the Migdal–Eliashberg theory of superconductivity [59–62]. When $w = (v_{kx} - v_{k'x})^2$, the function is called $\alpha_{tr}^2 F$. The weighted relaxation rate is defined correspondingly as

$$1/\tau_w = \frac{4\pi k_{\mathrm{B}} T}{\hbar} \int_0^\infty \frac{\mathrm{d}\Omega}{\Omega} \alpha_w^2 F(\Omega) \left[\frac{\hbar\Omega/2k_{\mathrm{B}}T}{\sinh(\hbar\Omega/2k_{\mathrm{B}}T)} \right]^2 \qquad (68)$$

When $w = 1$ this is the electron–phonon contribution to the Fermi surface average quasiparticle equilibration rate (except stripped of the renormalization factor $(1 + \lambda)^{-1}$). When $w = (v_{kx} - v_{k'x})^2$, it gives the electron–phonon part of $1/\tau_{tr}(T)$ which determines the resistivity in variational approximation. Numerical computations show that for elemental metals (see the inset of Fig. 6 for the case of In [63]; for Cu see ref. [58]) the various functions $\alpha_w^2 F(\Omega)$ bear a close resemblance to the phonon density of states $F(\Omega)$. Finally, we define dimensionless coupling constants λ_w by the equation

$$\lambda_w = 2 \int_0^\infty \frac{\mathrm{d}\Omega}{\Omega} \alpha_w^2 F(\Omega) \qquad (69)$$

The case $w = 1$ gives the coupling constant λ which determines the superconducting transition temperature of conventional metals [64,65]. At high T $(T > \Theta_D))$, relaxation rates $1/\tau_w \to 2\pi\lambda_w k_B T/\hbar$ are determined by the constants λ_w.

Quite a few calculations have been made of the superconducting function $\alpha^2 F(\Omega)$ and λ, but fewer of the corresponding transport function $\alpha_{tr}^2 F$. Shown in Fig. 7 are calculations [66] for four metals, done without adjustment of parameters. Agreement with experiment is at the 10% level. These calculations predate the development of efficient methods for calculating phonon dispersion ω_Q [67–69]. Therefore, ω_Q was taken from fits to experiment. The potential $\partial V/\partial u_\ell$ which determines the matrix element $M(kk')$ was not calculated self-consistently, but approximated as the rigid shift of the local "muffin-tin" potential. These approximations are appropriate for elemental metals only. Fully self-consistent calculations, using theoretical phonon curves, were reported for 8 metals in a monumental paper by Savrasov and Savrasov [70], for In in a careful study by
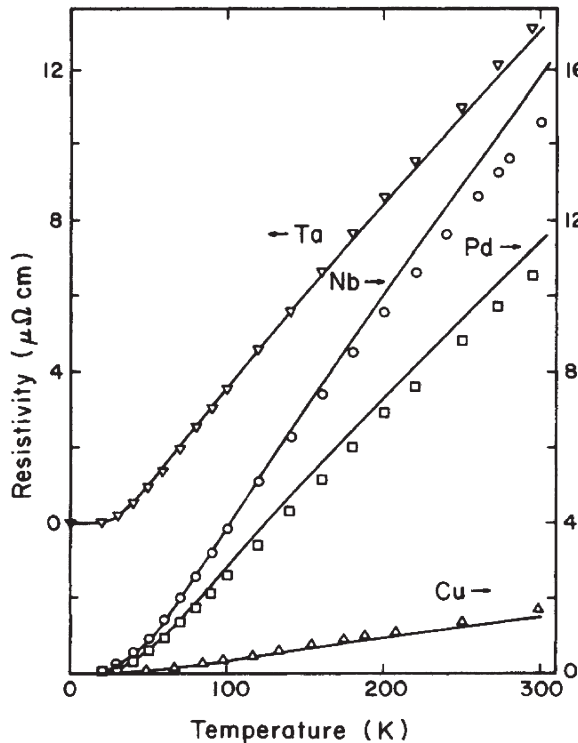

Fig. 7. Electrical resistivity of four transition metals versus temperature, showing experiment compared with computations. The calculations used experimental phonon dispersion curves and electronic band theory with no adjustable parameters as discussed in the text. See Allen et al. (1986) [66] and references therein.

Rudin et al. [63] shown in Fig. 6, and for 4 metals in an ambitious paper by Bauer et al. [71]. A result from Ref. [71] is shown later in Section 10.

Modern "first-principles" theory permits calculations for more complicated cases. The superconducting functions have been calculated for $SrCuO_2$ [72] and for MgB_2 [73–76a]. The latter material has very anisotropic electron–phonon scattering as k varies around the Fermi surface. Analogous to the known variation of the superconducting gap Δ_k is the variation of the shift τ_k Eq. (50) which fixes the non-equilibrium distribution function. One should expect significant k-dependence in τ_k for MgB_2, so the resistivity should deviate from the simplest variational approximation with constant τ_k. This in turn should give big deviations from Matthiessen's rule. The effect has been seen experimentally and explained by Mazin et al. [76b]. There are few serious attempts to calculate the electron-phonon resistivity of metals related to La_2CuO_4. There are two reasons: (1) metallic behavior is found only after doping which is an added challenge to theory; (2) there is doubt on the applicability of Landau Fermi liquid theory.

6.5. More Phenomenological Treatments

In Bloch's original work [4,77], an approximate formula emerged which Grüneisen [78] popularized. This "Bloch–Grüneisen" formula is just our variational result, evaluated for a spherical Fermi surface and a Debye phonon spectrum. It can be written as

$$\rho_{BG} = \rho_0 + \frac{16\pi^2 \lambda_{tr}\omega_D}{4\pi(n/m)_{eff}e^2} \left(\frac{2T}{\Theta_D}\right)^5 \int_0^{\Theta_D/2T} dx \frac{x^5}{\sinh^2 x} \qquad (70)$$

where the denominator of the prefactor, $\omega_P^2 = 4\pi(n/m)_{eff}e^2$ defines the "Drude" plasma frequency. For many metals this formula gives an excellent fit to the resistivity, with three adjustable parameters. The residual resistivity ρ_0 shifts the resistivity up and down. The Debye temperature Θ_D stretches the T axis. Finally, the strength of the electron–phonon part of the resistivity is fixed by the parameter λ_{tr}/ω_P^2. It would be desirable to obtain separate values of λ_{tr} and ω_P^2. In principle, ac measurements (see Eq. (6)) should be able to give the necessary extra information. Unfortunately, this is rarely the case. The biggest problem is that interband transitions often overlap the Drude region very severely. The case of Cu shown in Fig. 1 is far more benign than most. Another difficulty is that infrared-active vibrational modes appear in the spectrum of most interesting compound metals, complicating the fitting. For quite a few metals it has been shown that the Drude plasma frequency ω_P^2 given by density functional theory (DFT) [79] agrees remarkably well with experiment. This allows determination of an empirical value of λ_{tr} [80] provided the resistivity fits well to the Bloch–Grüneisen formula, and provided the theoretical ω_P^2 is known.

Non-cubic metals have anisotropic resistivities ($\rho_{xx} \neq \rho_{zz}$) which, according to Eq. (54) can arise both from anisotropy in $(n/m)_{eff}$ or in τ_{tr}, Eqs. (53) and (66). The similarity of λ_{tr} to λ shows that in many metals, there is little correlation between

velocities v_{kx} and matrix elements $I_{k,k'}$. Therefore we expect τ_{tr} to be fairly isotropic, and this agrees with experiment for metallic elements [81].

6.6. Quasiparticles from Band Theory

It is well established that DFT with good exchange-correlation potentials does surprisingly well for ground state properties, including vibrational spectra, but fails to give band gaps for higher energy excitations. At higher $\hbar\omega$, $\sigma(\omega)$ probes band gaps. Not only at higher ω, but also in the dc limit, calculations of σ should use quasiparticle energy bands [82] rather than DFT bands. However, experience shows that low-lying quasiparticle excitations of metals are very similar to DFT eigenvalues, for no known reason. Shapes of Fermi surfaces were predicted accurately well before the modern era of fully self-consistent DFT bands, and continue to be well described by DFT theory. Presumably they are not extremely sensitive to the potential. Group velocities are critical to accurate transport calculations. The isotropic average Drude plasma frequency squared can be written as $(e^2/3\pi^2\hbar)\int dA_k|\mathbf{v}_k|$, where dA_k is an element of Fermi-surface area. The ratio λ_{tr}/Ω_p^2 determines the magnitude of σ in a metal. Using $\lambda_{tr} \approx \lambda$ for metals where λ is accurately known from superconducting tunneling spectroscopy, the fitted Ω_p^2 agrees well with the DFT value. We can conclude that $\mathbf{v}_{k,DFT}$ agrees with $\mathbf{v}_{k,QP}$ for these metals [80]. Therefore at present, DFT eigenstates seem sufficient for transport theory.

6.7. Resistivity of High T_c-Superconductors

Figure 8 shows the temperature-dependence of electrical resistivity of two of the most famous high T_c compounds. The samples are believed to be extremely good [83,84]. Theoretical understanding is limited; transport phenomena in 3d metals still has surprises. For pure $YBa_2Cu_3O_7$, the data, on carefully detwinned samples, show "metallic" resistivity in all three crystallographic directions. The large magnitude of ρ (somewhat bigger than most conventional metals) can be assigned to the small carrier density. There is a factor of 2 anisotropy between the a-axis (lower resistivity) and b-axis. This was predicted before the experiment by DFT calculations of the Drude plasma frequency tensor $\Omega_{p\alpha\beta}$ [85], using the assumption that τ_{tr} is isotropic. Along the b-axis, where the CuO chains run, DFT gives $\hbar\Omega_p \approx 4.4\,\text{eV}$, while perpendicular to the chains, on the a-axis, it is $2.9\,\text{eV}$. The squared ratio agrees nicely with experiment. The c-axis anisotropy is not so well predicted. The calculated c axis plasma frequency of $1.1\,\text{eV}$ predicts ρ_c/ρ_b to be 7, while experiment gives 33. One might conclude that band theory works surprisingly well, as is also seen in photoemission spectroscopy.

On the other hand, part (b) of Fig. 8 shows what happens when holes are removed from optimally Sr-doped La_2CuO_4. Similar results are seen in $YBa_2Cu_3O_7$ [84]. At higher T, the nominally insulating samples have "metallic" ($d\rho/dT > 0$) resistivities. When the carrier density is scaled out, giving the inverse mobility $ne\rho$,
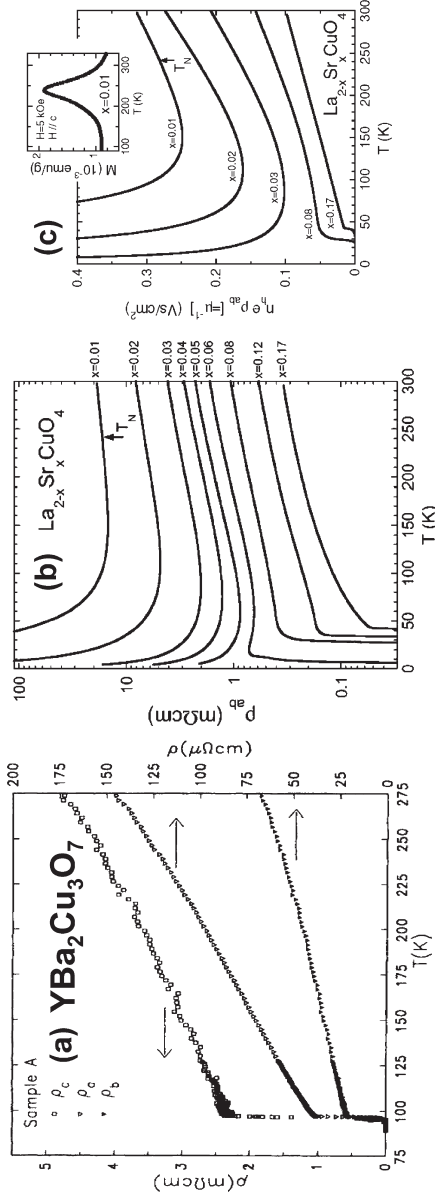
Fig. 8. Resistivity versus temperature of high T_c compounds. Part (a) shows the anisotropic resistivity of a detwinned single crystal of YBa$_2$Cu$_3$O$_7$ (from Friedmann et al., 1990 [83]). Part (b) shows the in-plane resistivity of a series of single crystals of La$_{2-x}$Sr$_x$CuO$_4$, with hole doping x going from a small x antiferromagnet to an optimum x superconductor (from Ando et al., 2001 [84]). (c) The same data (from Ando et al., 2001 [84]) on a linear scale after dividing out the nominal carrier density to get inverse mobility. The inset shows the Néel transition of the $x = 0.01$ sample detected as a peak in magnetization.

the mobilities of even antiferromagnetic "insulators," with 0.01 holes per unit cell, are only smaller than the mobilities of the optimum superconductor by a factor of 3. This strongly contradicts conventional notions that electrons in good metals behave ballistically, but dilute carriers in antiferromagnets have frustrated mobilities [86].

Whatever theory accounts for the optimum superconductor should therefore also account for the far under-doped antiferromagnet. The shape of $\rho(T)$ for the optimal superconductors is close to linear. A simple explanation is that this agrees with the Bloch–Grüneisen formula. The lower temperature region, where $\rho_{BG}(T)$ deviates from linear, is hidden from sight by superconductivity. However, this explanation does not work for under-doped materials. Also, the estimated mean-free path is too small at the more resistive end to justify quasiparticle transport [87]. The Hall coefficient has unusual temperature-dependence. The conclusion is that these data are still not understood.

7. KONDO EFFECT AND RESISTIVITY MINIMUM IN METALS

Figure 9 [88] shows resistivity of Au before and after implanting 60 ppm Fe impurities. The small resistivity upturn at low T has captured a huge amount of
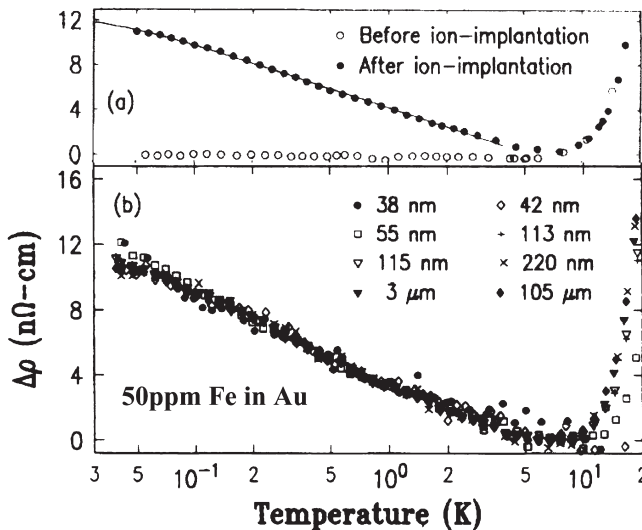

Fig. 9. Kondo resistivity [88]. The high-purity gold films used here are about 30 nm thick and have size-limited residual resistivities of order $\rho_0 \approx 2\,\mu\Omega\,cm$. At 300 K, phonon scattering contributes an additional $\rho - \rho_0 \approx 2\,\mu\Omega\,cm$. At temperatures shown here, the phonon scattering term is unobservable below 8 K, and its turn-on can be seen in the interval $8\,K < T < 20\,K$. After Fe implantation, a new T-dependent Kondo term $\Delta\rho \approx A - B\ln[1 + (T/\Theta)^2]$ is seen, whose magnitude is about 0.005 times ρ_0 and is independent of wire width (after subtracting an impurity-enhanced electron–electron contribution).

attention. The minimum in $\rho(T)$ at around 8 K is the crossover between phonon scattering causing $\rho(T)$ to increase with T at high T, and magnetic impurity scattering causing $\rho(T)$ to decrease with T at low T.

Anderson [89] showed how a transition metal impurity can either retain or lose its local magnetic moment when dissolved in a metal. Kondo [90,91] first glimpsed the complexity of the behavior when the moment is retained. The relevant part of the Hamiltonian is

$$H_{\text{Kondo}} = -\sum_{i,\ell} J(\mathbf{r}_i - \mathbf{R}_\ell)\sigma_i \cdot \mathbf{S}_\ell \tag{71}$$

where the ith electron of spin σ_i has a spin-flipping interaction with the ℓ'th magnetic impurity with spin $\mathbf{S}_\ell$. Perturbation theory for spin-flipping interactions differs from ordinary potential scattering from non-magnetic impurities in having a time-dependent impurity spin. For any time-dependent perturbation in a metal, the sharpness of the Fermi distribution causes logarithmic singularities in integrals. These diminish with T at least as fast as $\log(\varepsilon_{\text{F}}/k_{\text{B}}T)$ because of blurring of the Fermi distribution. An exact solution was found by Wilson [92,93] using the renormalization group, and by Andrei [94] using the Bethe Ansatz. These solutions were given a physical interpretation by Nozieres [95,96]. The subject is by no means closed. In particular, newer experimental tools applied to nanosystems permit more detailed exploration [97]. Finite biases in tunnel junctions allow the "Kondo resonance" to be explored by inelastic spectroscopy [98].

8. DIRTY FERMI LIQUIDS AND INTRINSICALLY DIFFUSIVE STATES

The Bloch–Boltzmann equation works beyond the naive expectation that weak interactions are required. However, the mean-free path of electrons in metals can often be reduced below 10 Å, where the definition of the wavevector of a quasiparticle is fuzzy. Metallic dirty alloys, liquids, and glasses are in this category. The other requirements for Fermi liquid status may still apply – there are complicated single-particle states of charge $\pm e$, spin $\pm\frac{1}{2}$, and energies sharp on a scale of ε_{F}. Because there is no wavevector, spectroscopies such as photoemission or Fermi-surface resonant techniques are not available to prove the value of this picture, but disorder does not automatically destroy the single-particle picture.

Dirty alloys are simplest, since the locations of atoms are known. Figure 10 shows an example [99]. In the region of (x, T) with $\rho < 125\,\mu\Omega\,\text{cm}$, $\rho(T)$ curves merge if shifted vertically – Matthiessen's rule is obeyed. When $\rho > 125\,\mu\Omega\,\text{cm}$, it is violated, but Boltzmann theory can no longer possibly be valid, because quasiparticles have had their k-vectors destroyed by either thermal disorder (in the pure V metal) or alloy disorder. In this regime, resistivity varies more weakly with (x, T) than when resistivity is smaller and quasiparticles exist. This phenomenon is called "resistivity saturation" after the paper by Fisk and Webb [100], and has been recently reviewed by Gunnarsson et al. [101–104].

First let us focus on $T = 0$. Theory should give reliable alloy disorder resistivity, because this is not a many-body problem. There are two limits. If the disorder is extremely large, states at the Fermi level may be Anderson-localized. Then the material will be insulating, meaning that as $T \to 0$, $\rho(T) \to \infty$. This is especially important in 2D disordered films, outside the scope of this article. In $d = 3$, localization is harder to achieve. Section 11 will discuss the metal-insulator transition in 3d-doped semiconductors, where Anderson localization does occur. Since the localized option occurs in $d = 3$, and since localization cannot be found by perturbation theory starting with delocalized basis functions, it is good to use a non-perturbative approach for resistivity of dirty alloys, such as exact diagonalization of finite subsamples. However, Brown et al. [105] showed that the "coherent potential approximation," a self-consistent perturbation theory, agrees with non-perturbative methods for at least one very dirty alloy.

For dirty 3d metals, as in Fig. 10, $\rho(T)$ shows reduced T-dependence. The dirtiest alloys ($V_{0.67}Al_{0.33}$) have a small negative $d\rho/dT$. There is no well-accepted explanation. Since $\rho(T)$ does not diverge at low T, true (or "strong") localization has not set in; the alloy is still a metal. Relatively few $d = 3$ metallic systems can be driven to the localized non-metallic state. Examples are $Ge_{1-x}Au_x$ [106,107] for small Au concentration $x \leqslant 0.12$, in both polycrystalline and amorphous films, and similarly
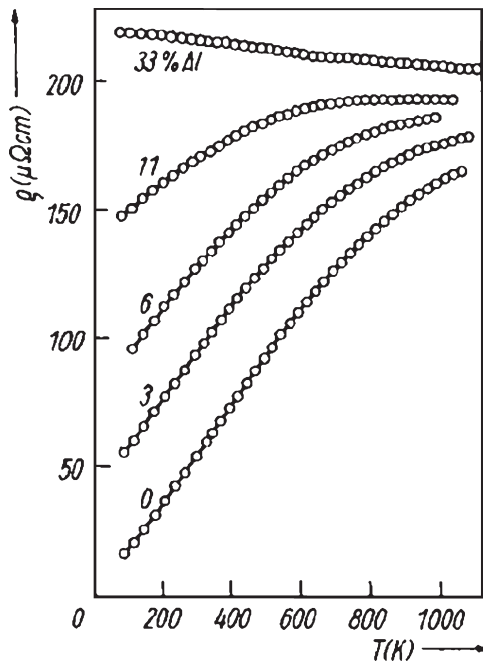

Fig. 10.   Electrical resistivity of $Ti_{1-x}Al_x$ alloys versus temperature [99]. Matthiessen's rule (the total resistivity is intrinsic plus a constant upward shift from impurity scattering) is well obeyed whenever $\rho < 125 \, \mu\Omega \, cm$. At larger resistivities, "saturation" is seen.

$Si_{1-x}Nb_x$ [108] for $x \leqslant 0.115$. It is necessary to make a heavy dilution of a metal like gold in a non-metal like Ge or Si, in order to get an insulator. At low T (below 20 K), a small upturn of $\rho(T)$ with decreasing T is often found, caused by effects beyond Boltzmann theory. If the effect is enhanced by disorder, then it is not a Kondo effect, but is denoted "weak localization" or "quantum corrections." Their origin is similar to the origin of Anderson or "strong" localization, but the resistivity remains well under $1000\,\mu\Omega$ cm, and the net change between 20 and 0 K is a few percent or less. These effects are discussed in Section 9.

There is an incorrect belief that $k_F\ell \approx 1$ or $\ell \approx a$ is the criterion for localization in 3d. Experiment clearly shows that this is not true, and that instead, metallic resistivity $100\,\mu\Omega$ cm $< \rho < 1000\,\mu\Omega$ cm (indicating $k_F\ell \approx 1$) occurs commonly with no sign of a true insulator. What is the mechanism of transport? Here is a thought experiment which could be computationally implemented on a large computer. For good crystalline metals, the propagating nature of Bloch states is proved by constructing Gaussian wavepackets out of $\mathbf{k}$-states centered on particular wavevectors $\mathbf{k}_0$. The Schrödinger equation evolves the state in time, the center of the wavepacket moving with the group velocity $\mathbf{v}_{\mathbf{k}0}$. This excitation transports charge and spin ballistically. Because of inevitable impurities, after a sufficiently long time ($t > \tau_k$) the wavepacket degrades and the center of charge stops moving. The squared width of the wavepacket continues to spread as $\langle r^2 \rangle \propto 3Dt$, where D is the diffusion constant, $D = v_k^2 \tau_k / 3$. Diffusion continues until the sample boundary is reached. A $d = 1$ computer experiment has been published for the case of weak disorder [109]. One dimension has the extra feature that the diffusion does not last forever, but evolves finally into localization with $\langle r^2 \rangle$ constant. In $d = 2$ the same effect should occur at extremely long times and distances, but lies beyond the power of computer experiment for weak disorder.

Consider the same construction in $d = 3$. The wavepacket should be built from eigenstates in a narrow energy window of the *delocalized* part of the spectrum of a very dirty metal, but the phases should be adjusted so that the resulting packet is spatially localized at $t = 0$. The time evolution is then computed, and it is found that $\langle r^2 \rangle \propto 3Dt$ starts immediately and holds to the boundaries, with $D \approx \hbar a^2 / W$ where W is the band-width of the metallic energy band ($\hbar/W$ is the time to hop to a nearest neighbor). One should experiment with the phases of the different component eigenstates trying to create a propagating packet. The effort will fail; no packet can be made that shows ballistic propagation; The states of the dirty metal are "intrinsically diffusive" and do not propagate ballistically farther than an interatomic distance. Therefore one cannot define a mean free path, but if forced to make a choice, one would have to say $\ell \approx a$. Such states are not teetering on the border of localization. They are generic in the spectrum of dirty metals. As you move in the one-electron spectrum toward a band gap, there is a "mobility edge" where $D \to 0$ and localization sets in. The localized states are a small minority and are far from the Fermi level in ordinary metals.

Exact calculations of ρ for dirty metals can be done in one-electron approximation from Eq. (25) if the eigenstates $|n\rangle$ are all known. If the states m, n are localized, then this formula will correctly give $\sigma = 0$, because whenever two states

are nearly degenerate, they will be separated spatially, with vanishing current matrix elements $\langle i|j_x|j\rangle = 0$. Successful calculations for alloys were reported by various groups [33–35,105,110,111].

Now return to $T > 0$. At high T, many relatively conventional crystalline metals show resistivities like those in Fig. 10 that deviate from the linear T-dependence predicted by Boltzmann theory. The reason is that the mean-free path ℓ has gotten too short (less than 10 Å). To see how electron–phonon interactions can give short mean-free paths, consider the lifetime broadening $\hbar/\tau = 2\pi\lambda k_B T$. Since λ is often of order 1, and $2\pi k_B T$ is 0.16 eV at room temperature, the levels are not necessarily narrower than the separation of adjacent bands. Consider Nb_3Sn, with $\lambda > 1$ and 8 atoms in a cubic unit cell. The total band width of the $4d$ levels is about 10 eV, and there are 30 d states in this band, for a mean level separation of 0.3 eV. Thus individual quasiparticle levels are not sharply defined. The resistivity [100] deviates strongly from the Bloch–Grüneisen form at room temperature. Although we understand why the theory fails, a useful theory to fix it [101–104,112] is not easily constructed.

9. WEAK LOCALIZATION AND QUANTUM CORRECTIONS

A huge range of fascinating low T transport effects goes under the various names "weak localization", or "mesoscopic fluctuations", or "interaction effects" or "quantum corrections." These effects show up as small corrections when resistivities are, large, but can be more significant when samples are small, especially in $d = 1$ or 2. An example is shown in Fig. 11 [113]. Quantum coherence is not just a property of well-organized propagating Bloch states where coherence is easily predictable. All solutions of t-independent Schrödinger equations are coherent. Components of a wavefunction interfere with other components of a superposition state. The coherence is only destroyed by t-dependent environmental perturbations such as scattering by phonons. Let $\hbar/\tau_{inel}$ be the lifetime broadening of a single-particle state caused by an environmental inelastic process. At low T, the scattering rate gets very small. Electrons therefore remain coherent for a long time, and may diffuse coherently over distances $L_{coh} = \sqrt{D\tau_{inel}}$ where the diffusion constant D is determined by elastic processes. In weakly disordered material, $D \approx v_F^2 \tau_{elast}$ while in strongly disodered systems the diffusion constant is a^2/τ_{hop} where τ_{hop} is the time to hop to a nearest neighbor a distance a away. This time is of order $\hbar/W$ where W is the band width. When the sample is smaller than L_{coh}, large "mesoscopic" fluctuations can be expected. The same wavefunction coherence is required for a single-particle state to become Anderson-localized. This is why quantum coherency corrections are called "weak localization" even though the system may be very far from true localization. Electron–electron Coulomb interactions also become enhanced at low T by the effects of disorder. For perfect Bloch states, Coulomb interactions are suppressed by Fermi degeneracy, $\hbar/\tau_C \approx \varepsilon_F (k_B T/\varepsilon_F)^2$. However, if the propagation is diffusive, two electron states, close enough to interact with each other, see the same pattern of disorder and tend to propagate similarly, giving an
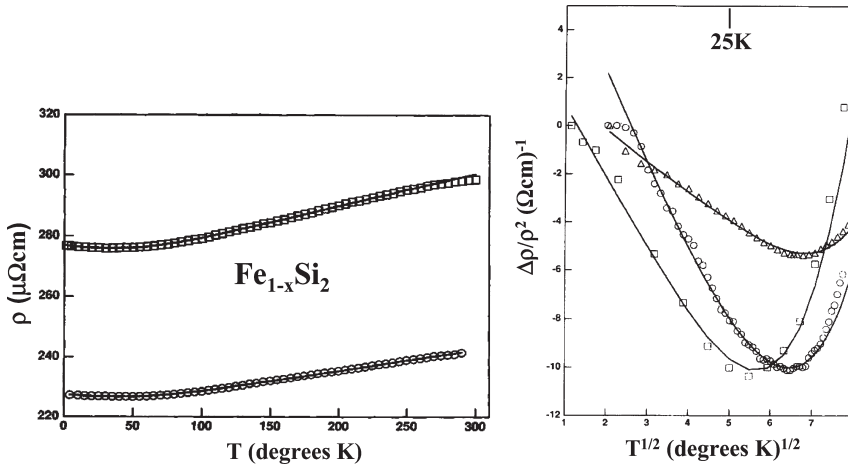
Fig. 11. Absolute (left) and relative (right) resistivity versus temperature for polycrystalline iron-deficient α-FeSi$_2$ films of thickness 100 nm (circles), 70 nm (squares), and 35 nm (triangles) [113]. The reduced and possibly saturated T-dependence characteristic of dirty metals is seen at $T > 100$ K. At $T < 50$ K, at the level of 1% of the total ρ, there is an interesting T-dependent upturn obeying approximately the law $A - BT^{1/2}$, characteristic of weak localization effects in $d = 3$.

enhancement of the Coulomb interaction. When samples are fairly clean, the corrections to ballistic propagation are weak, and perturbative theories predict leading corrections [114]. These theories go beyond conventional Fermi liquid theory, and have been confirmed in numerous experimental tests.

10. NEUTRON, PHOTOEMISSION, AND INFRARED SPECTROSCOPIES

Although these spectroscopies are not normally classified as transport, in fact they can measure otherwise inaccessible transport properties. Consider the lifetime-broadening of a phonon, as seen in infrared, Raman, or neutron scattering. The line shape formula is a spectral function analogous to the one defined for electrons in Eqs. (44), (45) and (48). On expects a broadened Lorentzian line shape, with broadening (full width at half maximum) Γ_Q of the normal mode Q given by 2 times the imaginary part of the corresponding phonon Green's function (see Fig. 12). This is a transport property. The phonon distribution obeys a Boltzmann equation written first by Peierls [115]. After linearizing, there is a rate of change due to collisions of the phonon distribution function

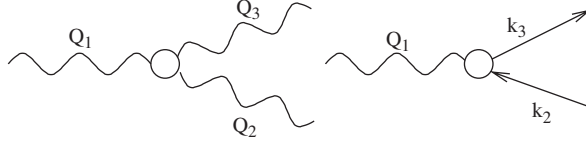$$\left(\frac{\partial N_Q}{\partial t}\right)_{\text{coll}} = -\sum_{Q'} I(Q, Q')\delta N_{Q'} \qquad (72)$$

Fig. 12. The phonon (wiggly line) can decay into two phonons by the third-order anharmonic coupling V_{123} or into an electron-hole pair by the electron–phonon coupling M_{123}.

If the only normal mode out of equilibrium is the mode Q, then the right-hand side is just $-I(Q,Q)\delta N_Q = -\Gamma_Q \delta N_Q$ and the population N_Q returns to equilibrium $n_Q = [\exp(\hbar\omega_Q/k_B T) - 1]^{-1}$ exponentially with time constant $1/\Gamma_Q$. By the usual arguments of time-dependent perturbation theory used to construct scattering terms in Boltzmann equations, one finds the formulas

$$\Gamma_1^{\text{anh}} = \frac{\pi}{\hbar^2} \sum_{23} |V_{123}|^2 [(n_2 + n_3 + 1)\delta(\omega_1 - \omega_2 - \omega_3) + 2(n_2 - n_3)\delta(\omega_1 + \omega_2 - \omega_3)]$$

(73)

$$\Gamma_1^{\text{ep}} = \frac{2\pi}{\hbar} \sum_{23} |M_{123}|^2 (f_2 - f_3)\delta(\hbar\omega_1 + \varepsilon_2 - \varepsilon_3)$$ (74)

where $1, 2, \ldots$ are short for $Q_1, Q_2, \ldots$. Here f and n are the equilibrium Fermi-Dirac and Bose–Einstein distributions, $\hbar\omega$ and ε are the phonon and electron quasiparticle energies, and V_{123} and M_{123} are the matrix elements for phonon–phonon scattering (third-order anharmonicity) and phonon–electron scattering, each being restricted by crystal momentum conservation (Q_1 must have the same wavevector *modulo* a reciprocal lattice vector as $Q_2 + Q_3$ or $k_3 - k_2$). The anharmonic matrix element V_{123} involves $(\partial^3 V_N/\partial u_1 \partial u_2 \partial u_3)A_1 A_2 A_3$, where A_i is the amplitude factor $\sqrt{\hbar/2M\omega_i}$ of the ith normal mode, and V_N the total nuclear potential energy (the same order of magnitude as ε_F). The second derivative $\partial^2 V_N/\partial u_1 \partial u_2$ is of order $M\omega^2$ where M is the nuclear mass. By counting factors appearing in these equations, one can determine that the order of magnitudes are

$$\Gamma_1^{\text{anh}}/\omega_{\text{ph}} = 2\pi |V_{123}|^2 F(\omega_{\text{ph}})n_{\text{ph}} \approx \frac{k_B T}{V_N}$$ (75)

$$\Gamma_1^{\text{ep}}/\omega_{\text{ph}} = 2\pi |M_{123}|^2 F(\omega_{\text{ph}})n_{\text{pairs}} \approx \frac{\hbar\omega_{\text{ph}}}{\varepsilon_F}$$ (76)

where $F(\omega_{\text{ph}})$ is the average phonon density of states, approximately $1/\hbar\omega_{\text{ph}}$. These equations use the previously mentioned size estimate $M(kk') \approx \sqrt{\varepsilon_F \hbar\omega_{\text{ph}}}$ and the corresponding estimate $V_{123} \approx \sqrt{(\hbar\omega_{\text{ph}})^3/V_N}$. Thus, we see that the two decay modes for phonons are roughly the same size. An important difference is that Γ_{anh} increases linearly with T at higher temperature, while Γ_{ep} is roughly independent of temperature. Other details affect the magnitude quite a lot. The electron–phonon process depends on $n_{\text{pairs}} \approx (N(0)\hbar\omega)^2$, the number of electrons and holes within a
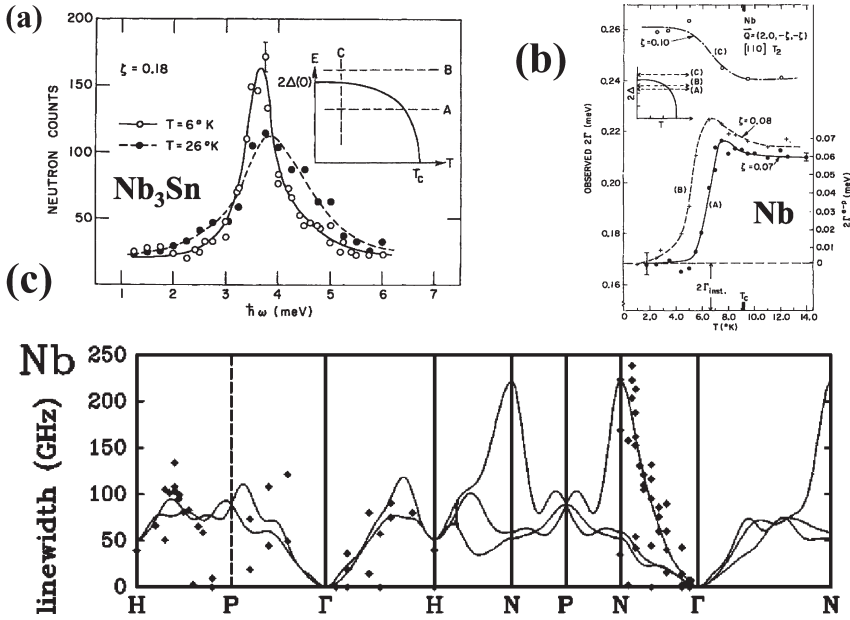
Fig. 13. (a) Change (for $T > T_c$ and $T < T_c$) of the line shape detected by neutrons for an acoustic phonon in the superconductor Nb_3Sn (from Axe and Shirane, [117]). (b) Measured line width as a function of T for various acoustic phonons in Nb (from Shapiro and Shirane, [116]). (c) Theoretical [71] and experimental [118] phonon line widths for Nb.

phonon energy ω of the Fermi energy. Different metals have quite different densities of states $N(0)$ at the Fermi energy – Pb and Nb differ by a factor of 3 (0.50 states/eV atom for Pb, 1.46 for Nb [7]) which appears squared in the phonon decay rate. Shapiro et al. [116–118] were able to see the extra broadening of Nb phonons caused by decay to electron-hole pairs, partly by exploiting the change in Γ when the superconducting transition occurs (see Fig. 13). Habicht et al. [119], using neutron echo techniques, saw no evidence for the electron-hole decay channel in Pb, consistent with a 10 times smaller expected electron decay relative to Nb, and a stronger anharmonic interaction.

Can we similarly measure electron equilibration rates $1/\tau_k$? Both photoemission and infrared spectroscopy provide partial measurements. In photoemission, electrons are ejected from a clean surface into vacuum where energy and wavevector are measured. Since the energy and wavevector of the incident photon are known, subtraction gives the energy and wavevector of the hole that was left behind, allowing mapping of energy bands. Two complications make the process less ideal. (1) The kosher theory of the process shows that a higher-order Green's function is needed [47,48]. (2) Since translational invariance is broken, crystal momentum k_z perpendicular to the surface is not conserved in the emission process – the sample can absorb arbitrary amounts of perpendicular momentum. This complicates the process of mapping bands and broadens the lineshapes. This second complication is
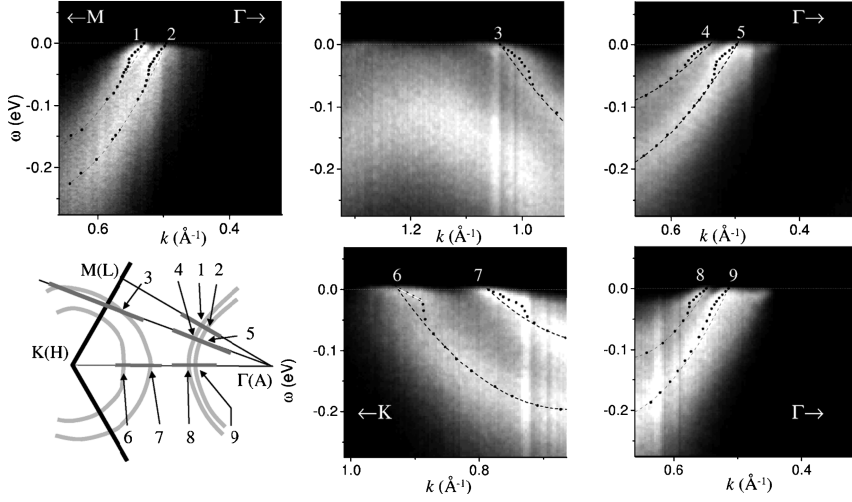
Fig. 14. Energy versus wavevector distributions of hole spectral weight (coded by color in the original [120]) seen in photoemission spectroscopy of the layered metal 2H-NbSe$_2$. The wavevector scans include nine Fermi surface crossings. Near each crossing the hole dispersion curve has a self-energy shift $-\omega\lambda_k(\omega)$, and the shift decreases at larger ω, leaving a kink in the dispersion curve which measures the size of λ_k. The values $\lambda_k \approx 0.85 \pm 0.15$ are deduced at all crossings except number 6 where the value 1.9 ± 0.2 is found.

eliminated if the hole lies in a surface state (**k** is 2d and has no z component) or lies in a quasi-2d band (ε_k depends very weakly on k_z). Figure 14 shows data [120] for 2H-NbSe$_2$, a quasi-2d metal with a strong electron–phonon interaction ($T_c = 7.2\,\mathrm{K}$). The energy resolution is 4–6 meV and k-resolution is $0.0025\,\mathring{\mathrm{A}}^{-1}$. Therefore, the intrinsic fuzziness of line shapes is larger than the resolution and reflects actual broadening and shifting of bands in $A(k, \omega)$. The data clearly show both broadening associated with Im Σ and a rapidly varying shift associated with ReΣ from electron–phonon interactions.

The lifetime broadening $1/\tau_k = -2\mathrm{Im}\,\Sigma$ can be found from Boltzmann theory using the diagonal part $k = k'$ of the linearized collision integral, Eq. (49). The answer is

$$\hbar/\tau_k = 2\pi \sum_{k'Q} |M(kk')|^2 [(1 - f_{k'} + n_Q) \times \delta(\varepsilon_k - \varepsilon_{k'} - \omega_Q)$$
$$+ (f_{k'} + n_Q)\delta(\varepsilon_k - \varepsilon_{k'} + \omega_Q)] \tag{77}$$

where $q = k - k'$. The alternate way to derive this is from the electron–phonon self-energy, for which, as shown by Migdal [121], perturbation theory behaves well. The self-energy to lowest order in the small parameter $\hbar\omega_{\mathrm{ph}}/\varepsilon_{\mathrm{el}}$ is

$$\Sigma(k, \omega) = \sum_{k'Q} |M(kk')|^2 \left(\frac{1 - f_{k'} + n_Q}{\omega + i\eta - \varepsilon_{k'} - \Omega_Q} + \frac{f_{k'} + n_Q}{\omega + i\eta - \varepsilon_{k'} + \Omega_Q} \right) \tag{78}$$

From the imaginary part evaluated at the band energy $\omega \to \varepsilon_k$, we get the same answer as in Boltzmann theory.

The consequences of the self-energy Eq. (78) have been seen experimentally in many metals, especially in superconducting tunneling experiments using planar junctions [122]. At low ω, Σ has the form $-\lambda_k\omega$. When λ_k is averaged over the Fermi surface, one gets the electron–phonon coupling constant λ which is of order 1 at low T. At higher excitation ω, λ goes to zero, which causes the kink seen in the near-Fermi-energy dispersion of Fig. 14.

Infrared spectroscopy is an alternate way to see the same physics as in planar tunneling junctions, and improvements in infrared sources and detectors make this method increasingly powerful. Holstein [123] argued that at infrared probing frequencies $\omega \sim \omega_{ph}$ there would be corrections to the Drude formula not contained in the ordinary low-frequency Boltzmann approximation. The starting point is Kubo's formula Eq. (16) for the conductivity,

$$\sigma(\omega) = \frac{i}{\omega}\left[r(\omega) + \frac{ne^2}{m}\right] \tag{79}$$

$$r(\omega) = i\int_0^\infty \mathrm{d}t\mathrm{e}^{\mathrm{i}\omega t}\langle[j(t), j(0)]\rangle \tag{80}$$

This formula can be evaluated only for simple systems without interactions. To get perturbative expressions for systems with interactions, a Wick-ordered $(\hat{T})$ imaginary time $(0 \leqslant \sigma \leqslant \beta = 1/k_BT)$ version of $r(\omega)$, is used, namely

$$r(\mathrm{i}\omega_\mu) = -\int_0^\beta \mathrm{d}\sigma \mathrm{e}^{\mathrm{i}\omega_\mu\sigma}\overline{\langle\hat{T}j(\sigma)j(0)\rangle} \tag{81}$$

$$r(\mathrm{i}\omega_\mu) = -\frac{e^2}{\beta}\sum_{kk'\nu} v_{k'x}\Gamma(kk', \mathrm{i}\omega_\mu, \mathrm{i}\omega_\nu)G(k, \mathrm{i}\omega_\nu + \mathrm{i}\omega_\mu)G(k, \mathrm{i}\omega_\nu) \tag{82}$$

$$G(k, \mathrm{i}\omega_\nu) = \frac{1}{\mathrm{i}\omega_\nu - \varepsilon_k - \Sigma(k, \mathrm{i}\omega_\nu)} \tag{83}$$

When analytically continued from the imaginary (Matsubara) frequencies $\mathrm{i}\omega_\mu = 2\pi\mu/\beta$ and $\mathrm{i}\omega_\nu = 2\pi(\nu + 1/2)/\beta$, with μ and ν integers, to just above the real frequency axis $\omega + \mathrm{i}\eta$ (η is infinitesimal), these functions become $r(\omega)$ as in Eq. (80) and G and Σ as in Eq. (44). The vertex function Γ is related to the self-energy Σ by a Ward's identity.

For electron–phonon systems, Holstein derived [22] the integral equation (generalized Boltzmann equation) for Γ at the Migdal level of approximation. Allen [124] showed that the resulting conductivity had the form

$$\sigma(\omega) = \frac{\mathrm{i}ne^2}{m\omega}\int_{-\infty}^\infty \mathrm{d}\omega' \frac{f(\omega') - f(\omega' + \omega)}{\omega - \Sigma_{ir}(\omega' + \omega + \mathrm{i}\eta) + \Sigma_{ir}^*(\omega' + \mathrm{i}\eta)} \tag{84}$$

The self-energy Σ_{ir} is almost exactly Σ of Eq. (78). The difference is in a k-dependent weighting factor $w(k, k')$, Eq. (67) similar to $(1 - \cos\theta_{kk'})$, that appears in the

Fermi-surface integration, and can be omitted to reasonable accuracy over much of the spectral range. Infrared experiments [125,126] have seen Holstein's predicted deviations from simple Drude behavior.

Unfortunately, Eq. (84) lacks the simplicity of the Drude form Eq. (6). Götze and Wölfle [127] suggested a simplified way to compute optical response in metals using peturbation theory for a "memory function" $M(\omega)$ defined as

$$\sigma(\omega) = \frac{ine^2/m}{\omega + M(\omega)} \qquad (85)$$

This is much closer to the Drude form, and in particular, the imaginary part of $M(\omega)$ is the generalization of the scattering rate $1/\tau$. Götze and Wölfle gave a closed formula for $M(\omega)$ at the lowest level of approximation. In the dc limit, their formula correctly reproduces the lowest-order variational solution of Boltzmann theory. Higher-order approximations for $M(\omega)$ are very messy, and the method is less reliable than Eq. (84). Infrared experiments, together with Kramers–Kronig analysis, can be used to extract $M(\omega)$, which is sometimes called an "optical single-particle self energy" [128]. An example is in Fig. 15, which shows interesting structure in $M(\omega)$ similar to what may be expected in a self-energy. Comparing
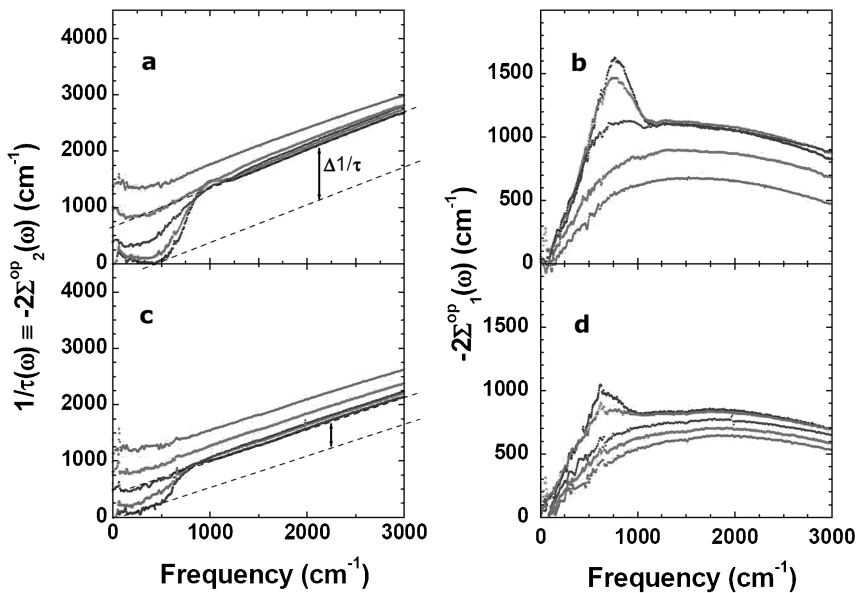

Fig. 15. Real (parts **b** and **d**) and imaginary (parts **a** and **c**) parts of the memory function $M = 2\Sigma^{op}$ measured by reflectance of untwinned single crystals of $Bi_2Sr_2CaCu_2O_{8+\delta}$, with optimal ($T_c = 96\,K$; parts **a** and **b**) and somewhat overdoped ($T_c = 82\,K$; parts **c** and **d**) oxygen concentrations [128]. Values are shown for five temperatures in each panel, namely, from bottom to top (left panels) and top to bottom (right panels), 27 K, 71 K, 101 K, 200 K, and 300 K.

Eqs. (84) and (85), one finds at low ω the relation

$$M(\omega) \sim -\omega \frac{\mathrm{dRe}\Sigma_{\mathrm{ir}}(\omega)}{\mathrm{d}\omega} - 2i\mathrm{Im}\,\Sigma_{\mathrm{ir}}(\omega) = \lambda_{\mathrm{ir}}\omega + i/\tau_{\mathrm{ir}} \qquad (86)$$

In the dc limit $M \to i/\tau_{\mathrm{ir}}$, the mass renormalization λ_{ir} disappears and the correct dc result is $ne^2\tau_{\mathrm{dc}}/m$, where τ_{dc} is the dc limit of τ_{ir}. Thus, in agreement with the semiclassical Boltzmann approach, the mass renormalization does not enter dc transport properties.

11. SEMICONDUCTORS AND THE METAL/INSULATOR TRANSITION

In semiconductors, carriers of electrical current are much more dilute than in metals. They are thermally activated out of filled bands, or injected by light, charged particles, or through tunnel barriers, or produced by intentional doping. Transport theory in semiconductors therefore differs from theory for metals. One main difference is that theory is often motivated by device applications [129], involving junctions and high fields, which takes us outside the linear ohmic regime [130]. Another difference is that dilute carriers and low temperatures opens up the fascinating insulator to metal transition. And a third difference is that hopping provides an alternate mechanism to band transport.

In a pure semiconductor, electrical transport occurs *via* thermally activated electron and hole carriers $n_{\mathrm{e}} = n_{\mathrm{h}} \propto \exp(-E_{\mathrm{g}}/2k_{\mathrm{B}}T)$, with E_{g} the gap between occupied valence and empty conduction bands. The conductivity σ is written as $n_{\mathrm{e}}e\mu_{\mathrm{e}} + n_{\mathrm{h}}e\mu_h$. The mobilities μ_{e} and μ_{h} of electron and hole carriers are typically quite large. Hall measurements provide values for the carrier density, and mobilities can be measured by drift velocity methods. In Si at $300\,\mathrm{K}$, electrons have $\mu_{\mathrm{e}} \approx 1.4 \times 10^3\,\mathrm{cm}^2/\mathrm{V\,s}$, and holes $\mu_{\mathrm{h}} \approx 4.5 \times 10^2\,\mathrm{cm}^2/\mathrm{V\,s}$ [131]. Experimental values of the temperature-dependent electron mobility are shown in Fig. 16 [132]. To explain these results [133] in detail requires solution of Boltzmann's equation, as discussed in a classic paper by Herring and Vogt [134], and performed by many authors using often Monte-Carlo procedures [132,135–137]. Silicon has electron carriers in 6 equivalent pockets, and holes in a heavy, a light, and a split-off hole band. One needs the scattering matrix elements for both intervalley and intravalley scattering by acoustic and optic phonons, making the total picture rather complex.

In doped semiconductors, the number of carriers no longer obeys $n_{\mathrm{e}} = n_{\mathrm{h}}$, but is determined by the temperature and the Fermi level which is fixed near the binding energy of the dominant impurity type. At higher temperatures, carriers of the majority type (electron or hole depending on whether doping is n- or p-type) are activated out of the impurity levels into band states which carry current by normal quasiparticle propagation. Scattering by ionized impurities now enters and often dominates.

At low temperatures, very interesting things happen to the transport properties of doped semiconductors. First consider lightly doped silicon. Fig. 17 shows the low T
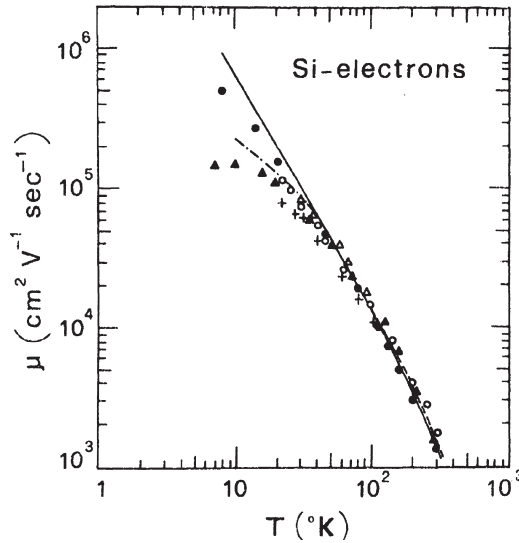
Fig. 16. Mobility versus temperature [132] for electrons in Si measured by time-of flight. The closed circles from Canali et al. used a very pure sample (donor and acceptor densities $\approx 10^{12}\,\mathrm{cm}^{-3}$), while earlier data shown by other symbols have impurity densities larger by up to 100, causing ionized impurity scattering to dominate at lower T. The power law $\mu \propto T^{3/2}$ from acoustic phonon scattering [133] is in rough accord, but the data do not have any simple power law.

conductivity of Si with 2.7×10^{17} phosphorus donor atoms per cm^3, and 0.8×10^{15} boron acceptors [138]. Notice how small the conductivity is. The value of σ closely follows $\exp(-12\,\mathrm{meV}/2k_\mathrm{B}T)$ until the temperature is lowered to a frequency-dependent point where the T-dependence becomes much weaker. Taking the dc limit, one sees that the conductivity below 2 K bends away from the activated line, to a weaker T-dependence. The mechanism for this tiny residual conductivity is hopping between localized impurity states. Most of the donor electrons are bound in hydrogenic localized orbitals with Bohr radius $\approx 14\,\mathrm{\mathring{A}}$, about 10 times smaller than the typical donor atom separation. However, because of the 300 times smaller concentration of boron acceptors, about 0.3% of the donor states become empty, the bound phosphorus electron recombining with a bound boron hole, leaving a P^+ and a B^- ion. The P^+ sites offer a place for a bound electron (on a neutral P) to hop to. This requires some non-zero thermal energy, because the donor P sites do not all have the same donor binding energy. Their energies are perturbed by Coulomb fields $e^2/\varepsilon R$ of the neighboring P^+ and B^- ions. At the dopant density of Fig. 17, this spatially fluctuating potential has characteristic size of several meV. Therefore there are empty higher energy sites and filled lower energy sites, separated by a Fermi level, and zero conductivity at $T = 0$. At finite temperature, random thermal fluctuations occur. The dominant fluctuation is hopping of isolated electrons back and forth between two nearby sites whose site energies happen to lie on either side of the Fermi level. These fluctuations couple to an oscillatory E field, giving an ac
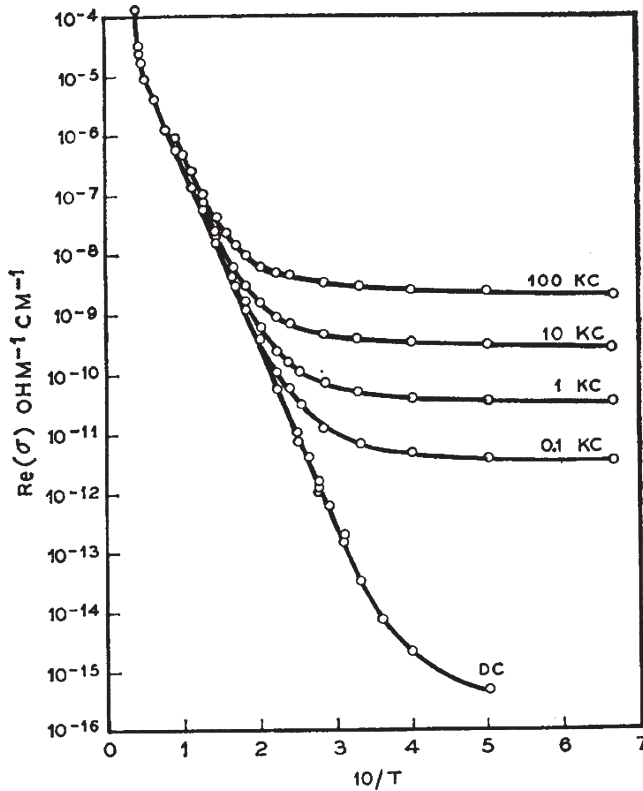
Fig. 17. Conductivity versus $10\,\mathrm{K}/T$ for Si with carrier density 10 times smaller than critical [138]. The linear slope comes from thermal activation out of the bound impurity states, and the strongly frequency-dependent low T limit comes from hopping.

conductance like a collection of random capacitors coupled by resistors. At a lower probability, there are longer range paths of electron propagation, giving a weakly activated hopping conduction which goes to zero as T goes to zero.

Mott [139] predicted successfully the form of the weakly activated hopping conduction, $\sigma_{\mathrm{VRH}} \propto \exp[-(T_0/T)^{1/4}]$, seen in many systems with localized charge carriers. The idea of "variable-range hopping" (VRH) is that the thermal energy $k_B T$ available to promote a hop may be too small to give a decent rate for nearby hops where wavefunctions $\psi \propto \exp(-\alpha r)$ have large overlap. Especially at low T, the hop may have to go to a farther neighbor with smaller overlap. A compromise is reached between the overlap $\exp(-2\alpha R)$ and the probability of available energy $\exp(-\Delta E(R)/k_B T)$ where $\Delta E(R)$ is the likely minimum energy hop available within a radius R of the starting point. This energy scales as $1/N(\varepsilon_F)R^3$. The optimum distance is found by minimizing the product by R, and gives a likely range $R_0 \propto [\alpha N(\varepsilon_F)k_B T]^{-1/4}$. Weakly activated hopping with $T^{1/4}$ is the result. Mott's arguments not only agree with many experiments [140] but have also been confirmed theoretically by various methods [141–143].
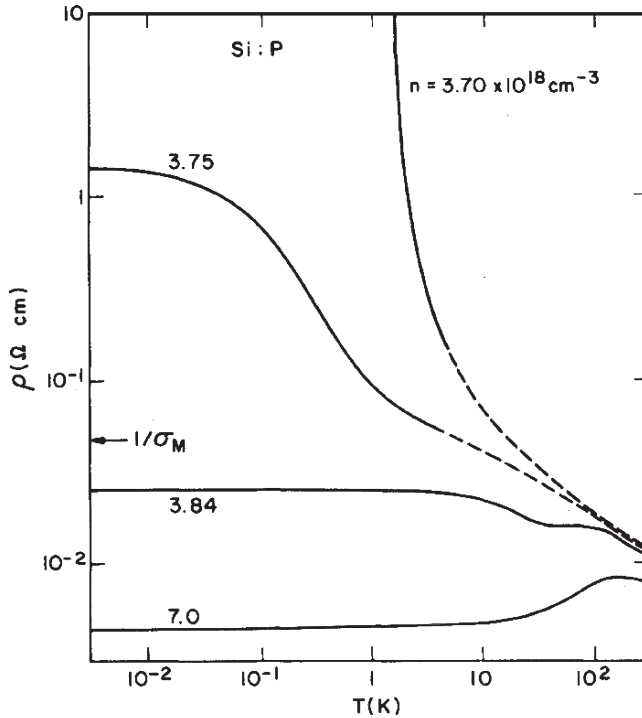
Fig. 18. Resistivity versus T of uncompensated Si, for four phosphorus concentrations near the critical concentration $\approx 3.75 \times 10^{18}\,\mathrm{cm}^{-3}$ [144].

Contrast this weak conductance at low doping with the measured resistivity shown in Fig. 18 [144] at phosphorus doping higher by 10. At a sharp critical donor concentration $n_c \approx 4 \times 10^{18}\,\mathrm{cm}^{-3}$ [145,146], where the average separation of localized impurity states drops to about 4 times the Bohr radius of these states, a continuous transition begins. Electron states at the Fermi level delocalize, and the $T = 0$ conductivity is no longer 0. The material is no longer insulating, and so must be called a "metal." This "Anderson transition" [147] is now known to occur in 3d but not in 1d where *all* states are localized no matter how weak is the disorder. The intermediate case of 2d is marginal and still controversial [148].

The transition from localized to delocalized is somewhat subtle, in that it does not show up in the single-particle density of states or in the single-particle Green's function averaged over a macroscopic system. Figure 19 [149] shows infrared spectra for three different doping levels, all below the critical concentration. At light doping, the hydrogenic impurity levels show up as lines in the infrared as expected. At heavier doping, it is perhaps not surprising that the lines are broadened by impurity overlap, which eliminates any sign of discrete levels at doping n 3 times below n_c. One might guess that the spectrum at the highest doping shown would indicate delocalized states, but dc conductivity shows otherwise – it goes to zero as T goes to zero, although at any achievable temperature it is far higher than the
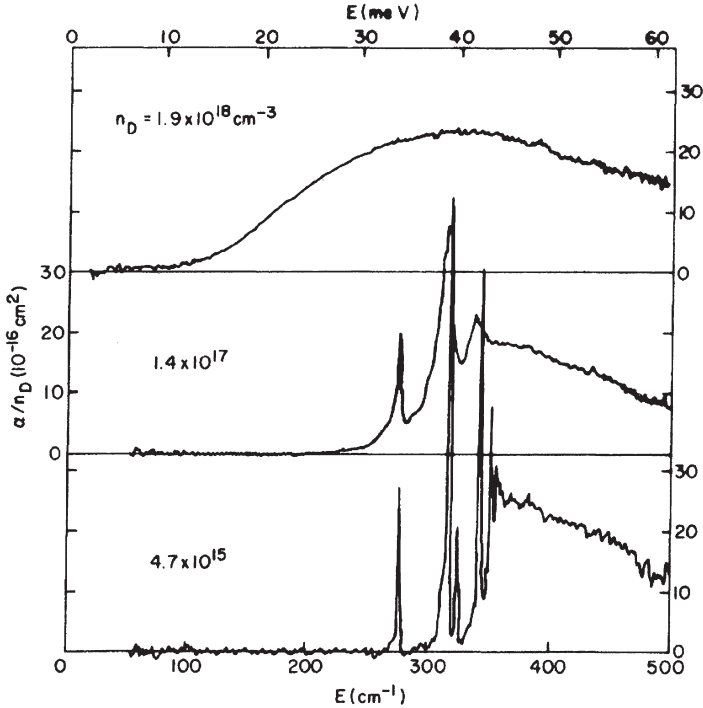
Fig. 19. Absorption coefficient α (in cm^{-1}) per donor (in cm^{-3}) measured at $T = 2\,K$ for uncompensated P-doped Si versus infrared photon energy [149]. Bound to bound impurity transitions are seen at the lowest doping, and broaden due to overlap of neighboring impurity states at heavier doping.

conductivity in Fig. 17 at 1.2 K. Before Anderson's paper, it was assumed that delocalization always occurred to some degree. After Anderson's paper was understood and generalized by Mott and others [150], a different picture emerged. The impurity levels are always localized when they are very dilute. As the concentration increases, overlapping pairs and clusters occur. The excited states of these dopant atoms overlap even more, and perhaps become delocalized, and probably merge with the unoccupied conduction band. However, the n_{imp} ground levels, which are distributed in energy by random perturbations, have the ability to resist delocalization, at least in the lower energy part of their spectrum. Somewhere higher in the spectrum there is necessarily a sharply defined energy ε_c, called the "mobility edge," which separates localized from delocalized states. The insulator to metal transition occurs when the mobility edge coincides with the Fermi level. The measured resistivity [151] at very low T is plotted in Fig. 20 for a series of samples across this transition.

It is also known [152,153] that Coulomb interactions between electrons have important consequences for the metal/insulator transition. Many of the experimental studies have been on "uncompensated" samples where only one species of
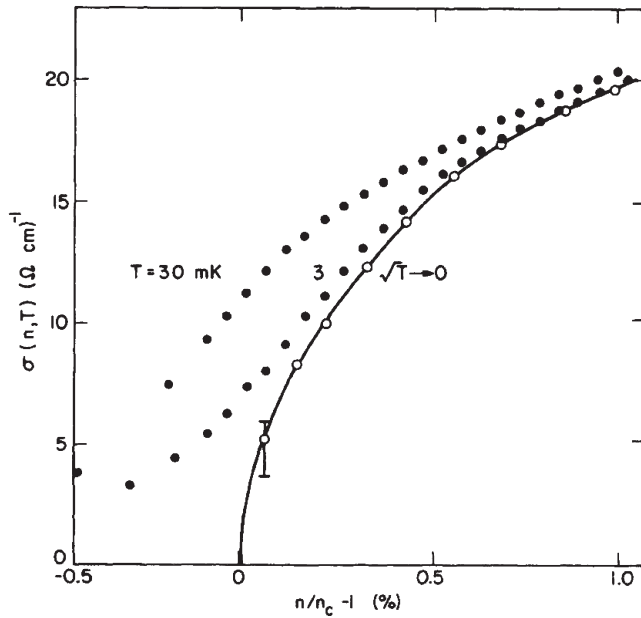
Fig. 20. Conductivity versus dopant density at two temperatures (30 and 3 mK) plus (open circles) the extrapolation to $T = 0$ assuming a $\sqrt{T}$ law [151]. The curve is a fit with critical exponent $v = 1/2$. The measurements are all on the same sample, with dopant density changes simulated by varying the applied stress.

dopant occurs. ("Compensated" means that both n and p type dopants occur.) At low and uncompensated doping and $T = 0$, all dopant levels are singly occupied. There are no ionized impurity atoms, and no doubly occupied impurity levels because of the significant on-site repulsion, comparable to the binding energy. As doping increases and dopant levels start to overlap, the transition to metallic conduction may be more like a Mott transition [154,155], dominated by correlations, instead of an Anderson transition, dominated by disorder. This is still a fascinating and controversial subject. The data of Fig. 20 show a critical exponent $\sigma(T = 0) \propto (n/n_c - 1)^v$ with $v \approx 1/2$. The theory of the pure Anderson transition (with no Coulombic electron–electron interactions) predicts v to be close to 1. When samples are intentionally compensated, most experiments seem to show an exponent closer to 1, as is also seen in diluted metals like Nb_xSi_{1-x} [108]. However, the data are not necessarily good enough close to the transition to measure the critical exponent [156].

12. COULOMB BLOCKADE

Coulomb interactions alter transport properties in many ways. In homogeneous 3d metals, little influence is seen in low-frequency transport, apart from screening all

interactions and thus affecting the single-particle spectrum. Electron–phonon or impurity scattering overpower Coulomb scattering as a relaxation mechanism, owing to the Pauli principle which suppresses Coulomb scattering by $(k_B T/\varepsilon_F)^2$ as shown in Section 6.3.

More dramatic Coulomb effects are seen at low T in special situations, of which the simplest is the "Coulomb blockade" of electron tunneling. Consider a case such as Fig. 4 or 21c, with electrons tunneling through a small conducting island separated from both leads by tunnel barriers. The addition of a single electron to the island raises the electrostatic energy of the island by $\Delta U_I = e^2/2C_{eff}$ where C_{eff} is the total island capacitance. A gate electrode coupled to the island capacitively with capacitance C_g and gate potential V_g, can raise and lower the energy of this added electron by $\Delta U_g = e(C_g/C_{eff})V_g$. If (1) source-drain bias V_{SD}, (2) temperature $k_B T$, and (3) single-particle electron level spacing $\Delta\varepsilon_I$ on the island, are all small compared to ΔU_I, conductance through the island is suppressed. The suppression is periodically modulated by the gate. Whenever the gate voltage is tuned so that the energy for adding one electron aligns with the source and drain electrode Fermi level, the conductance peaks. This happens periodically with spacing $\Delta V_g = e/C_g$, and corresponds to successive increases of the island's net electron charge. These effects in the single-particle tunneling regime were predicted by Averin and Likharev [157] and seen first by Fulton and Dolan [158]. The device is called a "single-electron transistor," and an "orthodox theory" [159] gives accurate fits to data. When the island level spacing $\Delta\varepsilon_I$ is small compared with $k_B T$, a simple theoretical expression due to Kulik and Shekhter [160] applies,

$$G = G_{max} \frac{\Delta U/k_B T}{\sinh(\Delta U/k_B T)} \tag{87}$$

where $\Delta U = \Delta U_g - \Delta U_I$ and $1/G_{max} = 1/G_1 + 1/G_2$ is the peak conductance, with G_1 and G_2 the conductances of the tunnel barriers to the source and drain electrodes.

Figure 21(a and b) shows the conductance versus gate voltage for a junction of metallic Al electrodes and an Al island (size $\approx (40\,\text{nm})^3$) separated by an aluminum oxide tunnel barrier [161]. The conductance peak G_{max} is smaller by 100 than the quantum unit $G_0 = 2e^2/h$ seen in the ballistic point contact, Fig. 3. This indicates that tunneling rather than ballistic conductance is occurring. The level spacing of Al valence states in such an island is $\approx 3\,\text{mK}$, less than the temperatures used (400, 200, and 6 mK in panel (a), and 300, 200, 100, and 50 mK in panel (b)). The data on panel (b) fit very well to the theory of Averin et al. [162] which extends the formula of Kulik and Shekhter to include "cotunneling," a higher-order process where tunneling across both barriers is coordinated, leaving an electron-hole pair on the island. This process increases with T quadratically as the phase space for the electron-hole pairs increases. Figure 21d, for a smaller Al island [163], shows the more complete story for source drain voltages which are no longer small compared with the other energies, and when finite level spacing due to island size quantization starts to set in.
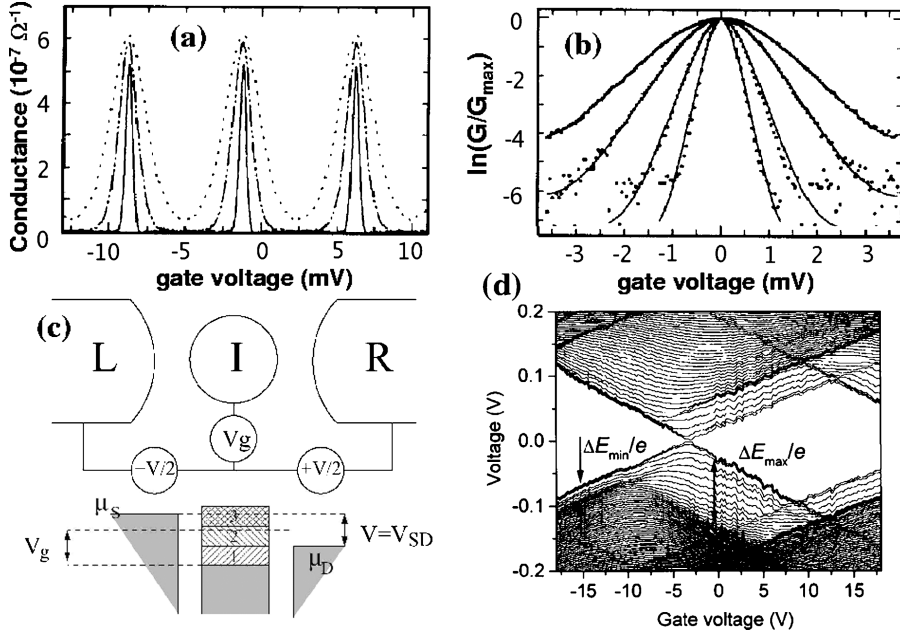
Fig. 21. Coulomb blockade of electron tunneling through a metallic Al island separated by oxide from Al electrodes [161,163]. Panels (a) and (b), for small source-drain voltage $V_{SD} = V$, show conductance versus gate voltage at various temperatures: from top to bottom, T = 400 mK, 200 mK, and 6 mK in (a), and T = 300 mK, 200 mK, 100 mK, and 50 mK in (b). The linear conductance peaks whenever the gate voltage is tuned to a point where one more electron can hop onto the island without increase of energy. This is indicated in the schematic diagram (c) where the energy levels of the island are denoted as continua with different discrete island Fermi levels corresponding to additional electrons $1, 2, 3$ on the island. For infinitesimal V_{SD}, conductance is shut off unless the Fermi level of the island for some change state n aligns with the source and drain chemical potentials μ_S, μ_D. Panel (d) shows data at 4.2 K for a very small island. The lines are contours of constant current in increments of 50 pA. Data of panels a and b (on bigger islands) correspond to the horizontal line $V = V_{SD} = 0$. At constant but non-zero V_{SD}, current can flow for a non-zero interval of gate voltage. The width of this interval increases with V_{SD} giving diamond-shaped openings of blocked current. Fine structure is caused by energy level discreteness on the island.

13. COULOMB GAP

Important but more subtle effects of the Coulomb interaction are seen in systems near a metal to insulator transition, and appear as a suppression of electron density of states $N(\varepsilon)$ for small $|\varepsilon - \mu|$ where μ is the Fermi level. Efros and Shklovskii [152] found that $N(\varepsilon)$ vanishes as $|\varepsilon - \mu|^p$ with $p \approx 2$ when the Fermi level lies on the insulating side of the transition. Altshuler and Aronov [153] and McMillan [164] found a cusp-like suppression, $N(\varepsilon) = N(\varepsilon_F)[1 + (|\varepsilon - \mu|/\delta)^{1/2}]$ when ε_F lies on the metallic side. Tunneling conductance of boron-doped silicon near the metal
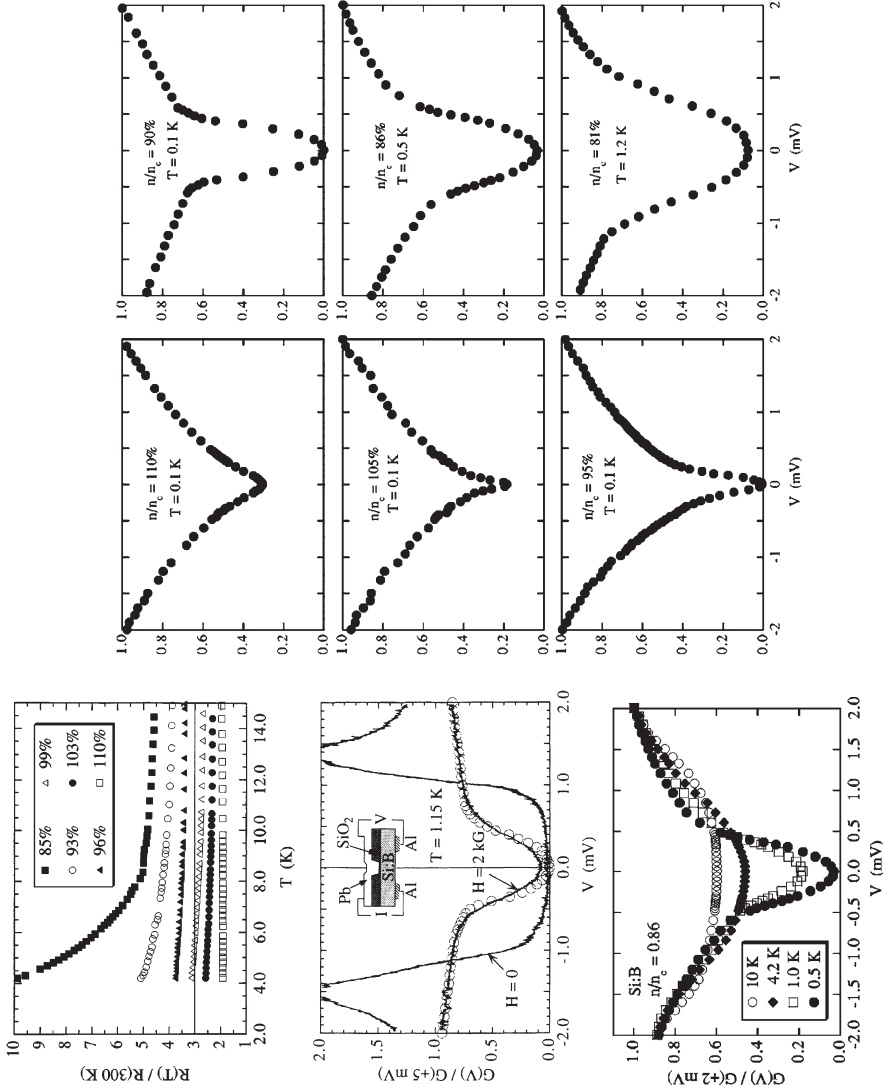
Fig. 22. Coulomb gap in boron-doped silicon at concentrations near the metal to insulator transition [165–167]. Upper left: Resistance versus T for six samples with various dopings n/n_c with $n_c = 4 \times 10^{18}$ cm^{-3} the critical concentration. Middle left: $H = 0$ conductance shows the gap of the Pb electrodes, verifying that junctions do exhibit tunneling. Six panels on right: Conductance, intepreted as thermally smeared density of states with a cusp in the metallic samples and a soft Coulomb gap in the insulating samples. Lower left: By 10 K, the anomaly is gone and all samples look rather similar.

insulator transition at $n_c = 4 \times 10^{18}$ cm^{-3} measured by Lee et al. [165–167], shown in Fig. 22, confirm these ideas. In the tunneling regime, with a barrier height large compared to bias voltage, the tunneling conductance $G(V)$ is proportional to the thermally broadened density of states $\int d\varepsilon N(\varepsilon) \partial f(\varepsilon - eV)/\partial V$. Very similar effects were seen for amorphous Nb$_x$Si$_{1-x}$ near the metal to insulator transition at $x =$ 0.115 by Hertel et al. [108].

   On the insulating side, the nearly complete depletion for ε near μ is called a "soft" Coulomb gap. The explanation by Efros and Shlovskii is very simple. Suppose there are localized electron states at random positions $\mathbf{R}_i$, with a random distribution of energies h_i, before adding the Coulomb repulsion between the electrons which will occupy some of these sites. For each occupied pair, there is a repulsive energy $v_{ij} = e^2/\kappa R_{ij}$ where κ is the dielectric constant and R_{ij} the distance. The problem is to find the stable occupancy assuming fewer electrons than sites. The energy to remove one electron, leaving the rest fixed, is $\xi_i = h_i + \sum_j v_{ij} n_j$ where n_j is the occupancy of site j. The energy to add one more electron in a previously empty state is $\xi_k = h_k + \sum_j v_{kj} n_j$. The density of states is

$$N(\varepsilon) = -\frac{1}{\pi} \sum_i \mathrm{Im}\, G(i, \varepsilon) = \sum_i \delta(\varepsilon - \xi_i) \tag{88}$$

where the single particle removal energy is used for $\xi < \mu$ and the single particle addition energy for $\xi > \mu$, as is usual for the spectral density of states defined from the Green's function, and measured in the tunneling experiment. Efros and Shklovski point out that the energy difference Δ between the N particle ground state and the excited state with state i removed and state j added is $\xi_j - \xi_i - v_{ij}$. Although the first part $\xi_j - \xi_i$ is positive, the second part is negative, and it is not obvious that the sum is positive for small $|\xi_j - \xi_i|$. In fact, the only way to guarantee that Δ is always positive is for the ground state occupancy to be organized such that the states ξ_i are depleted near μ.

   The Altshuler–Aronov argument for the cusp on the metal side is quite different, and relies on being able to compute perturbatively around the metallic state with good Fermi-liquid behavior and no disorder. Thus, there is no evident reason why the theoretically predicted anomalies on the two sides of the transition should be related. Experiment shows forcefully the unity of the phenomena. For $T \geqslant 10$ K (shown in panel (a) of Fig. 22) the resistivity does not distinguish insulator from metal. Tunneling conductances measured at low T show $N(\varepsilon)$ recovering rapidly from the low ε anomaly and behaving similarly for metal and insulator. It is reminiscent of the resistivity of high T_c superconductors in Fig. 8, which at higher T look similar for metal and insulator [84], defying theory.

ACKNOWLEDGMENTS

REFERENCES

[1] P. Drude, Zur Elektronentheorie der Metalle, *Ann. Phys. (Leipzig) Ser.* **4**(1), 566–613 (1900).

[2] A. Sommerfeld, Zur elektronentheorie der metalle auf grund der fermischen statistik, *Zeits. and Physik* **47**, 1–32 and 43–60 (1928).

[3] A. Sommerfeld and H. Bethe, Elektronentheorie der Metalle, *Handbook Phys.* **24/2**, 1–290 (1932).

[4] F. Bloch, Über die quantenmechanik der elektronen in kristallgittern, *Zeits. Phys.* **52**, 555–600 (1928).

[5] L.D. Landau, Oscillations in a fermi liquid, *J. Exp. Theor. Phys.* **30**, 1058 (1956), engl. transl. in *Men of Physics: L. D. Landau I*, edited by D. ter Haar, (Pergamon, Oxford, 1965), pp. 105–118.

[6] P.B. Johnson and R.W. Christy, Optical constants of copper and nickel as a function of temperature, *Phys. Rev. B* **11**, 1315–1323 (1975).

[7] D.A. Papaconstantopoulos, *Handbook of the Band Structure of Elemental Solids* (Plenum, New York, 1986).

[8] J.C. Maxwell, *A Treatise on Electricity and Magnetism*, Dover, New York.

[9] Y.V. Sharvin, A possible method for studying Fermi surfaces, *Sov. Phys. JETP* **21**, 655 (1965).

[10] G. Wexler, Size effect and non-local Boltzmann transport equation in orifice and disk geometry, *Proc. Phys. Soc. London* **89**, 927 (1966).

[11] B. Nikolic and P.B. Allen, Electron transport through a circular constriction, *Phys. Rev. B* **60**, 3963–3966 (1999).

[12] B.J. van Wees, H. van Houten, C.W.J. Beenakker, J.G. Williamson, L.P. Kouwenhoven, D. van der Marel and C.T. Foxon, Quantized conductance of point contacts in a two-dimensional electron gas, *Phys. Rev. Lett.* **60**, 848–850 (1988).

[13] B.J. van Wees, L.P. Kouwenhoven, E.M.M. Willems, C.J.P.M. Harmans, J.E. Mooij, H. van Houten, C.W.J. Beenakker, J.G. Williamson and C.T. Foxon, Quantum ballistic and adiabatic electron transport studied with quantum point contacts, *Phys. Rev. B* **43**, 12431–12453 (1991).

[14] D.A. Wharam, T.J. Thornton, R. Newbury, M. Pepper, H. Ahmed, J.E.F. Frost, D.G. Hasko, D.C. Peacock, D.A. Ritchie and G.A.C. Jones, One-dimensional transport and the quantisation of the ballistic resistance, *J. Phys. C* **21**, L209–L214 (1988).

[15] R. de Picciotto, H.L. Störmer, L.N. Pfeiffer, K.W. Baldwin and K.W. West, Four-terminal resistance of a ballistic quantum wire, *Nature* **411**, 51–54 (2001).

[16] M.A. Topinka, B.J. LeRoy, S.E.J. Shaw, E.J. Heller, R.M. Westervelt, K.D. Maranowski and A.C. Gossard, Imaging coherent electron flow from a quantum point contact, *Science* **289**, 2323–2326 (2000).

[17] R. Kubo, Statistical mechanical theory of irreversible processes. I. General theory and simple applications to magnetic and conduction problems, *J. Phys. Soc. Jpn.* **12**, 570–586 (1957).

[18] G. Rickayzen, *Green's Functions and Condensed Matter* (Academic Press, London, 1980).

[19] G.D. Mahan, *Many Particle Physics (Physics of Solids and Liquids)*, 3rd ed. (Kluwer Academic, 2000).

[20] G.M. Eliashberg, Transport equation for a degenerate system of Fermi particles, *Sov. Phys. JETP* **14**, 886–892 (1962).

[21] R.E. Prange and L.P. Kadanoff, Transport theory for electron–phonon interactions in metals, *Phys. Rev.* **134**, A566–A580 (1964).

[22] T.D. Holstein, Theory of transport phenomena in an electron–phonon gas, *Ann. Phys.* **29**, 410–535 (1964).

[23] J.M. Ziman, *Models of Disorder* (Cambridge University Press, Cambridge, 1979).

[24] D.A. Greenwood, The Boltzmann equation in the theory of electrical conduction in metals, *Proc. Phys. Soc.* **71**, 585–591 (1958).

[25] R. Landauer, Spatial variation of currents and fields due to localized scatterers in metallic conduction, *IBM J. Res. Dev.* **1**, 223–331 (1957), **32**, 306–316 (1988).

[26] D.S. Fisher and P.A. Lee, Relation between conductivity and transmission matrix, *Phys. Rev. B* **23**, 6851–6854 (1981).

[27] S. Datta, *Electronic Transport in Mesoscopic Systems* (Cambridge University Press, Cambridge, 1995).

[28] H. Haug and A.-P. Jauho, *Quantum Kinetics in Transport and Optics of Semiconductors* (Springer, 1996).

[29] Y. Imry and R. Landauer, Conductance viewed as transmission, *Rev. Mod. Phys.* **71**, S306–S312 (1999).

[30] Y. Meir and N.S. Wingreen, Landauer formula for the current through an interacting electron region, *Phys. Rev. Lett.* **68**, 2512–2515 (1992).

[31] C. Caroli, R. Combescot, P. Nozieres and D. Saint-James, Direct calculation of the tunneling current, *J. Phys. C: Sol. State Phys.* **4**, 916–929 (1971).

[32] D. Kalkstein and P. Soven, A Green's function theory of surface states, *Surf. Sci.* **26**, 85–99 (1971).

[33] T.N. Todorov, Calculation of the residual resistivity of three-dimensional quantum wires, *Phys. Rev. B* **54**, 5801–5813 (1996).

[34] B.K. Nikolic and P.B. Allen, Resistivity of a metal between the Boltzmann transport regime and the Anderson transition, *Phys. Rev. B* **63**, 020201:1–4 (2001).

[35] Y. Gilman, J. Tahir-Kheli, P.B. Allen and W.A. Goddard III, Numerical study of resistivity of model disordered three-dimensional metals, *Phys. Rev. B* **70**, 224201:1–3 (2004).

[36] S. Datta, Nanoscale device modeling: The Green's function method, *Superlatt. Microstr.* **28**, 253–278 (2000).

[37] N.D. Lang and P. Avouris, Electrical conductance of individual molecules, *Phys. Rev. B* **64**, 125323:1–7 (2001).

[38] D.M. Adams, L. Brus, C.E.D. Chidsey, S. Creager, C. Creutz, C.R. Kagan, P.V. Kamat, M. Lieberman, S. Lindsay, R.A. Marcus, R.M. Metzger, M.E. Michel-Beyerle, J.R. Miller, M.D. Newton, D.R. Rolison, O. Sankey, K. Schanze, J. Yardley and X. Zhu, Charge transfer on the nanoscale: Current status, *J. Phys. Chem B* **107**, 6668–6697 (2003).

[39] A. Nitzan and M.A. Ratner, Electron transport in molecular wire junctions, *Science* **300**, 1384–1389 (2003).

[40] M. Brandbyge, J.-L. Mozos, P. Ordejn, J. Taylor and K. Stokbro, Density-functional method for nonequilibrium electron transport, *Phys. Rev. B* **65**, 165401:1–17 (2002).

[41] A.F. Andreev, The thermal conductivity of the intermediate state in superconductors, *Sov. Phys. JETP* **19**, 1228–1231 (1964).

[42] R.J. Soulen Jr., J.M. Byers, M.S. Osofsky, B. Nadgorny, T. Ambrose, S.F. Cheng, P.R. Broussard, C.T. Tanaka, J. Nowak, J.S. Moodera, A. Barry and J.M.D. Coey, Measuring the spin polarization of a metal with a superconducting point contact, *Science* **282**, 85–88 (1998).

[43] G.E. Blonder, M. Tinkham and T.M. Klapwijk, Transition from metallic to tunneling regimes in superconducting microconstrictions: Excess current, charge imbalance, and supercurrent conversion, *Phys. Rev. B* **25**, 4512–4532 (1982).

[44] Report of the investigation committee on the possibility of scientific misconduct in the work of Hendrik Schön and coauthors, Tech. rep., http://publish.aps.org/reports/lucentrep.pdf (2002).

[45] J. Yamashita and S. Asano, Electrical resistivity of transition metals I, *Prog. Theor. Phys.* **51**, 317–326 (1974).

[46] F.J. Pinski, P.B. Allen and W.H. Butler, Calculated electrical and thermal resistivities of Nb and Pd, *Phys. Rev. B* **23**, 5080–5096 (1981).

[47] W.L. Schaich and N.W. Ashcroft, Model calculations in the theory of photoemission, *Phys. Rev. B* **2**, 2452–2465 (1971).

[48] G.D. Mahan, Theory of photoemission in simple metals, *Phys. Rev. B* **2**, 4334–4350 (1970).

[49] J.M. Ziman, *Electrons and Phonons* (Oxford University Press, London, 1960), chap. VII.

[50] P.B. Allen, Boltzmann Theory and Resistivity of Metals, *in Quantum Theory of Real Materials* (Kluwer, Boston, 1996), chap. 17.

[51] L.D. Landau and E.M. Lifshitz, *Statistical Physics*, 3rd ed. part I (Pergamon Press, Oxford, 1980), sect. 55.

[52] P.B. Allen, Fermi surface harmonics: A general method for non-spherical problems. Application to Boltzmann and Eliashberg equations, *Phys. Rev. B* **13**, 1416–1427 (1976).

[53] P.B. Allen, New method for solving Boltzmann's equation for electrons in metals, *Phys. Rev. B* **17**, 3725–3734 (1978).

[54] P.B. Allen, Empirical electron–phonon λ values from resistivity of cubic metallic elements, *Phys. Rev. B* **36**, 2920–2923 (1987).

[55] V.F. Gantmakher and Y.B. Levinson, *Carrier Scattering in Metals and Semiconductors* (North-Holland, 1987).

[56] B. Raquet, M. Viret, E. Sondergard, O. Cespedes and R. Mamy, Electron–magnon scattering and magnetic resistivity in $3d$ ferromagnets, *Phys. Rev. B* **66**, 024433 (2002).

[57] J. Bass, Deviations from Matthiessen's rule, *Adv. Phys.* **21**, 431 (1972).

[58] T.P. Beaulac, P.B. Allen and F.J. Pinski, Electron–phonon effects in copper. II. Electrical and thermal resistivities and Hall coefficient, *Phys. Rev. B* **26**, 1549–1558 (1982).

[59] G.M. Eliashberg, Interactions between electrons and lattice vibrations in a superconductor, *Sov. Phys. JETP* **11**, 696–702 (1960).

[60] D.J. Scalapino, The electron–phonon interaction and strong-coupling superconductors, *Superconductivity* (M. Dekker, New York, 1969) chap. 10.

[61] P.B. Allen and B. Mitrović, Theory of superconducting T_c, *Solid State Physics* (Academic, New York, 1982) **37**, pp. 1–92.

[62] J.P. Carbotte, Properties of boson-exchange superconductors, *Rev. Mod. Phys.* **62**, 1027–1157 (1990).

[63] S.P. Rudin, R. Bauer, A.Y. Liu and J.K. Freericks, Reevaluating electron–phonon coupling strengths: Indium as a test case for *ab initio* and many-body theory methods, *Phys. Rev. B* **58**, 14511–14517 (1998).

[64] W. McMillan, Transition temperature of strong-coupled superconductors, *Phys. Rev.* **167**, 331–344 (1968).

[65] P.B. Allen and R.C. Dynes, Transition temperature of strong-coupled superconductors reanalyzed, *Phys. Rev. B* **12**, 905–922 (1975).

[66] P.B. Allen, T. Beaulac, F. Khan, W. Butler, F. Pinski and J. Swihart, dc transport in metals, *Phys. Rev. B* **34**, 4331–4333 (1986).

[67] S. Baroni, P. Giannozzi and A. Testa, Green-function approach to linear response in solids, *Phys. Rev. Lett.* **58**, 1861–1864 (1987).

[68] P. Giannozzi, S. de Gironcoli, P. Pavone and S. Baroni, *Ab initio* calculation of phonon dispersions in semiconductors, *Phys. Rev. B* **43**, 7231–7242 (1991).

[69] S. Baroni, S. de Gironcoli, A.D. Corso and P. Giannozzi, Phonons and related crystal properties from density-functional perturbation theory, *Rev. Mod. Phys.* **73**, 515–562 (2001).

[70] S.Y. Savrasov and D.Y. Savrasov, Electron–phonon interactions and related physical properties of metals from linear-response theory, *Phys. Rev. B* **54**, 16487–16501 (1996).

[71] R. Bauer, A. Schmid, P. Pavone and D. Strauch, Electron–phonon coupling in the metallic elements Al, Au, Na, and Nb: A first-principles study, *Phys. Rev. B* **57**, 11276–11282 (1998).

[72] S.Y. Savrasov and O.K. Andersen, Linear-response calculation of the electron–phonon coupling in doped $CaCuO_2$, *Phys. Rev. Lett.* **77**, 4430–4433 (1996).

[73] H.J. Choi, D. Roundy, H. Sun, M.L. Cohen and S.G. Louie, The origin of the anomalous superconducting properties of MgB_2, *Nature* **418**, 758–760 (2002).

[74] K.P. Bohnen, R. Heid and B. Renker, Phonon dispersion and electron–phonon coupling in MgB_2 and AlB_2, *Phys. Rev. Lett.* **86**, 5771–5774 (2001).

[75] J. Kortus, I.I. Mazin, K.D. Belashchenko, V.P. Antropov and L.L. Boyer, Superconductivity of metallic boron in MgB_2, *Phys. Rev. Lett.* **86**, 4656–4659 (2001).

[76] (a) T. Yildirim, O. Gulseren, J.W. Lynn, C.M. Brown, T.J. Udovic, Q. Huang, N. Rogado, K.A. Regan, M.A. Hayward, J.S. Slusky, T. He, M.K. Haas, P. Khalifah, K. Inumaru and R.J. Cava, Giant anharmonicity and nonlinear electron–phonon coupling in MgB_2 A combined first-principles calculation and neutron scattering study, *Phys. Rev. Lett.* **87**, 037001 (2001).

(b) I.I. Mazin, O.K. Andersen, O. Jepsen, O.V. Dolgov, J. Kortus, A.A. Golubov, A.B. Kuz'menko and D. van der Marel, Superconductivity in MgB_2: Clean or Dirty? *Phys. Rev. Lett.* **89**, 107002 (2002).

[77] F. Bloch, Zum elektrischen Widerstandsgesetz bei tiefen Temperaturen, *Z. Phys.* **59**, 208–214 (1930).

[78] E. Grüneisen, Die Abhängigkeit des elektrischen Widerstandes reiner Metalle von der Temperatur, *Ann. Phys. (Leipzig)* **4**, 530–540 (1933).

[79] W. Kohn and L.J. Sham, Self-consistent equations including exchange and correlation effects, *Phys. Rev* **140**, A1133–A1138 (1965).

[80] P.B. Allen, Electron–Phonon coupling constants, *Handbook of Superconductivity* (Academic Press, San Diego, 2000) pp. 478–489.

[81] B.A. Sanborn, P.B. Allen and D.A. Papaconstantopoulos, Empirical electron–phonon coupling constants and anisotropic electrical resistivity in hcp metals, *Phys. Rev. B* **40**, 6037–6044 (1989).

[82] L.J. Sham and W. Kohn, One-particle properties of an inhomogeneous interacting electron gas, *Phys. Rev.* **145**, 561–567 (1966).

[83] T.A. Friedmann, M.W. Rabin, J. Giapintzakis, J.P. Rice and D.M. Ginsberg, Direct measurement of the anisotropy of the resistivity in the a-b plane of twin-free, single-crystal, superconducting YBa$_2$Cu$_3$O$_{7-\delta}$, *Phys. Rev. B* **42**, 6217–6221 (1990).

[84] Y. Ando, A.N. Lavrov, S. Komiya, K. Segawa and X.F. Sun, Mobility of the doped holes and the antiferromagnetic correlations in underdoped high-T_c cuprates, *Phys. Rev. Lett.* **87**, 017001:1–4 (2001).

[85] P.B. Allen, W.E. Pickett and H. Krakauer, Anisotropic normal-state transport properties predicted and analyzed for high-T_c oxide superconductors, *Phys. Rev. B* **37**, 7482–7490 (1988).

[86] W.F. Brinkman and T.M. Rice, Single-particle excitations in magnetic insulators, *Phys. Rev. B* **2**, 1324–1338 (1970).

[87] M. Gurvitch and A.T. Fiory, Resistivity of La$_{1.825}$Sr$_{0.175}$CuO$_4$ and YBa$_2$Cu$_3$O$_7$ to 1100 K: absence of saturation and its implications, *Phys. Rev. Lett.* **59**, 1337–1340 (1987).

[88] V. Chandrasekhar, P. Santhanam, N.A. Penebre, R.A. Webb, H. Vloeberghs, C.V. Haesendonck and Y. Bruynseraede, Absence of size dependence of the Kondo resistivity, *Phys. Rev. Lett.* **72**, 2053–2056 (1994).

[89] P.W. Anderson, Localized magnetic states in metals, *Phys. Rev.* **124**, 41–53 (1961).

[90] J. Kondo, Resistance minimum in dilute magnetic alloys, *Progr. Theoret. Phys. (Kyoto)* **32**, 37–69 (1964).

[91] G. Grüner and A. Zawadowski, Magnetic impurities in non-magnetic metals, *Rep. Prog. Phys.* **37**, 1497 (1974).

[92] K.G. Wilson, The renormalization group: Critical phenomena and the Kondo problem, *Rev. Mod. Phys.* **47**, 773–840 (1975).

[93] H.R. Krishna-murthy, J.W. Wilkins and K.G. Wilson, Renormalization-group approach to the Anderson model of dilute magnetic alloys. I. Static properties for the symmetric case, *Phys. Rev. B* **21**, 1003–1043 (1980).

[94] N. Andrei, K. Furiya and J.H. Lowenstein, Solution of the Kondo problem, *Rev. Mod. Phys.* **55**, 331–402 (1983).

[95] P. Nozieres, A 'fermi-liquid' description of the Kondo problem at low temperatures, *J. Low. Temp. Phys.* **17**, 31–42 (1974).

[96] A.C. Hewson, *The Kondo problem to Heavy Fermions* (Cambridge University Press, Cambridge, 1997).

[97] K. Nagaoka, T. Jamneala, M. Grobis and M.F. Crommie, Temperature dependence of a single Kondo impurity, *Phys. Rev. Lett.* **88**, 077205 (2002).

[98] D. Goldhaber-Gordon, H. Shtrikman, D. Mahalu, D. Ambusch-Magder, U. Meirav and M.A. Kastner, Kondo effect in a single-electron transistor, *Nature* **391**, 156–159 (1998).

[99] J.H. Mooij, Electrical conduction in concentrated disordered transition-metal alloys, *Phys. Stat. Sol.* **a17**, 521–530 (1973).

[100] Z. Fisk and G.W. Webb, Saturation of the high-temperature. Normal-state electrical resistivity of superconductors, *Phys. Rev. Lett.* **36**, 1084–1086 (1976).

[101] O. Gunnarsson, M. Calandra and J.E. Han, Colloquium: Saturation of electrical resistivity, *Rev. Mod. Phys.* **75**, 1085–1099 (2003).

[102] M. Calandra and O. Gunnarsson, Electrical resistivity at large temperatures: Saturation and lack thereof, *Phys. Rev. B* **66**, 205105:1–20 (2002).

[103] M. Calandra and O. Gunnarsson, Violation of Ioffe-Regel condition but saturation of resistivity of the high-T_c cuprates, *Europhys. Lett.* **61**, 88–94 (2003).

[104] O. Gunnarsson and J.E. Han, The mean free path for electron conduction in metallic fullerenes, *Nature* **405**, 1027–1030 (2000).

[105] R.H. Brown, P.B. Allen, D.M. Nicholson and W.H. Butler, Resistivity of strong-scattering alloys: absence of localization and success of coherent-potential approximation confirmed by exact supercell calculations in $V_{1-x}Al_x$, *Phys. Rev. Lett.* **62**, 661–664 (1989).

[106] B.W. Dodson, W.L. McMillan, J.M. Mochel and R.C. Dynes, Metal-insulator transition in disordered Germanium-Gold alloys, *Phys. Rev. Lett.* **46**, 46–49 (1981).

[107] W.L. McMillan and J. Mochel, Electron tunneling experiments on amorphous $Ge_{1-x}Au_x$, *Phys. Rev. Lett.* **46**, 556–557 (1981).

[108] G. Hertel, D.J. Bishop, E.G. Spencer, J.M. Rowell and R.C. Dynes, Tunneling and transport measurements at the metal-insulator transition of amorphous Nb: Si, *Phys. Rev. Lett.* **50**, 743–746 (1983).

[109] P.B. Allen and J. Kelner, Evolution of a vibrational wavepacket on a disordered chain, *Am. J. Phys.* **66**, 497–506 (1998).

[110] R. Kahnt, The calculation of the resistivity of liquid and amorphous transition metals *via* the Landauer formula, *J. Phys. C: Condens. Matter* **7**, 1543–1556 (1995).

[111] R. Arnold and H. Solbrig, Disorder-induced resistivity of liquid and amorphous transition metals calculated within the scattered-wave supercell concept, *J. Non-Cryst. Solids* **205–207**, 861–865 (1996).

[112] P.B. Allen and B. Chakraborty, Infrared and d.c. conductivity in metals with strong scattering: non-classical behavior from a generalized Boltzmann equation containing band mixing effects, *Phys. Rev. B* **23**, 4815–4827 (1981).

[113] K.K. Larsen, M.V. Hove, A. Lauwers, R.A. Donaton, K. Maex and M.V. Rossum, Electronic transport in metallic iron disilicide, *Phys. Rev. B* **50**, 14200–14211 (1994).

[114] B.L. Altshuler, P.A. Lee and R.A. Webb (Eds), *Mesoscopic Phenomena in Solids* (North-Holland, Amsterdam, 1991).

[115] R.E. Peierls, On the kinetic theory of thermal conduction in crystals, *Ann. Phys. (Leipzig) Ser.* **5**(3), 1055–1101 (1929).

[116] S.M. Shapiro, G. Shirane and J.D. Axe, Measurements of the electron–phonon interaction in Nb by inelastic neutron scattering, *Phys. Rev. B* **12**, 4899–4908 (1975).

[117] J.D. Axe and G. Shirane, Influence of the superconducting energy gap on phonon linewidths in Nb_3Sn, *Phys. Rev. Lett.* **30**, 214–216 (1973).

[118] N. Wakabayashi, Phonon anomalies and linewidths in Nb at 10 K, *Phys. Rev. B* **33**, 6771–6774 (1986).

[119] K. Habicht, R. Golub, F. Mezei, B. Keimer and T. Keller, Temperature-dependent phonon lifetimes in lead investigated with neutron-resonance spin-echo spectroscopy, *Phys. Rev. B* **69**, 104301:1–8 (2004).

[120] T. Valla, A.V. Fedorov, P.D. Johnson, P.-A. Glans, C. McGuinness, K.E. Smith, E.Y. Andrei and H. Berger, Quasiparticle spectra, charge-density waves, superconductivity, and electron–phonon coupling in $2H-NbSe_2$, *Phys. Rev. Lett.* **92**, 086401:1:4 (2004).

[121] A.B. Migdal, Interaction between electrons and lattice vibrations in a normal metal, *Sov. Phys. JETP* **7**, 996–1001 (1958).

[122] W.L. McMillan and J.M. Rowell, Tunelling and Strong-Coupling Superconductivity, *Superconductivity* (M. Dekker, New York, 1969), chap. 11.

[123] T. Holstein, Optical and infrared volume absorptivity of metals, *Phys. Rev.* **96**, 535–536 (1954).

[124] P.B. Allen, Electron–phonon effects in the infrared properties of metals, *Phys. Rev. B* **3**, 305–320 (1971).

[125] R.R. Joyce and P.L. Richards, Phonon contribution to far-infrared absorptivity of superconducting and normal lead, *Phys. Rev. Lett.* **24**, 1007–1010 (1970).

[126] B. Farnworth and T. Timusk, Phonon density of states of superconducting lead, *Phys. Rev. B* **14**, 5119–5120 (1976).

[127] W. Götze and P. Wölfle, Homogeneous dynamical conductivity of metals, *Phys. Rev. B* **6**, 1226 (1972).

[128] J. Huang, T. Timusk and G. Gu, High transition temperature superconductivity in the absence of the magnetic resonance mode, *Nature* **427**, 714–717 (2004).

[129] S.M. Sze, *Physics of Semiconductor Devices*, 2nd ed. (Wiley, New York, 1981).

[130] E.M. Conwell, *High Field Transport in Semiconductors* (Academic, New York, 1967).

[131] See the electronic archive New Semiconductor Materials maintained at the Ioffe Institute: ⟨http://www.ioffe.rssi.ru/SVA/NSM/Semicond/⟩.

[132] C. Canali, C. Jacoboni, F. Nava, G. Ottaviani and A.A. Quaranta, Electron drift velocity in silicon, *Phys. Rev. B* **12**, 2265–2284 (1975).

[133] F. Seitz, On the mobility of electrons in pure non-polar insulators, *Phys. Rev.* **73**, 549–564 (1948).

[134] C. Herring and E. Vogt, Transport and deformation-potential theory for many-valley semiconductors with anisotropic scattering, *Phys. Rev.* **101**, 944 (1956).

[135] P. Norton, T. Braggins and H. Levinstein, Impurity and lattice scattering parameters as determined from Hall and mobility analysis in n-type silicon, *Phys. Rev. B* **8**, 5632–5646 (1973).

[136] L.R. Logan, H.H.K. Tang and G.R. Srinivasan, Analytic solutions to the Boltzmann equation for electron transport in silicon, *Phys. Rev. B* **43**, 6581 (1991).

[137] B.A. Sanborn, P.B. Allen and G.D. Mahan, Theory of screening and electron mobility: Application to n-type silicon, *Phys. Rev. B* **46**, 15123 (1992).

[138] M. Pollak and T.H. Geballe, Low-frequency conductivity due to hopping processes in silicon, *Phys. Rev.* **122**, 1742–1753 (1961).

[139] N.F. Mott, Conduction in non-crystalline materials: 3. localized states in a pseudogap and near extremities of conduction and valence bands, *Philos. Mag.* **19**, 835 (1969).

[140] M. Pollak and B. Shklovskii (Eds), Hopping Transport in Solids (North-Holland, New York, 1991).

[141] V. Ambegaokar, B.I. Halperin and J.S. Langer, Hopping conductivity in disordered systems, *Phys. Rev. B* **4**, 2612–2620 (1971).

[142] W. Brenig, G. Döhler and P. Wölfle, Theory of thermally assisted electron hopping in amorphous solids, *Z. Phys.* **246**, 1–12 (1971).

[143] M. Pollak, A percolation treatment of dc hopping conduction, *J. Non-Cryst. Solids* **11**, 1024 (1972).

[144] T.F. Rosenbaum, R.F. Milligan, M.A. Paalanen, G.A. Thomas, R.N. Bhatt and W. Lin, Metal–insulator transition in a doped semiconductor, *Phys. Rev. B* **27**, 7509–7523 (1983).

[145] U. Thomanschefsky and D.F. Holcomb, Metal–insulator transition in the compensated semiconductor Si: (P,B), *Phys. Rev. B* **45**, 13356–13362 (1992).

[146] P. Dai, Y. Zhang and M.P. Sarachik, Critical conductivity exponent for Si: B, *Phys. Rev. Lett.* **66**, 1914–1917 (1991).

[147] P.W. Anderson, Absence of diffusion in certain random lattices, *Phys. Rev.* **109**, 1492–1505 (1958).

[148] S.V. Kravchenko, G.V. Kravchenko, J.E. Furneaux, V.M. Pudalov and M. D'Iorio, Possible metal-insulator transition at B = 0 in two dimensions, *Phys. Rev. B* **50**, 8039–8042 (1994).

[149] G.A. Thomas, M. Capizzi, F. DeRosa, R.N. Bhatt and T.M. Rice, Optical study of interacting donors in semiconductors, *Phys. Rev. B* **23**, 5472 (1981).

[150] N.F. Mott, *Metal-Insulator Transitions* (Taylor and Francis, London, 1974).

[151] G.A. Thomas, M. Paalanen and T.F. Rosenbaum, Measurements of conductivity near the metal-insulator critical point, *Phys. Rev. B* **27**, 3897–3900 (1983).

[152] A.L. Efros and B.I. Shklovskii, Coulomb gap and low temperature conductivity of disordered systems, *J. Phys. C: Solid State Phys.* **8**, L49–L51 (1975).

[153] B.L. Altshuler and A.G. Aronov, Zero bias anomaly in tunnel resistance and electron–electron interaction, *Solid State Commun.* **30**, 115–117 (1979).

[154] D. Belitz and T.R. Kirkpatrick, The Anderson–Mott transition, *Rev. Mod. Phys.* **66**, 261–380 (1994).

[155] M. Imada, A. Fjimori and Y. Tokura, Metal-insulator transitions, *Rev. Mod. Phys.* **70**, 1039–1263 (1998).

[156] H.v. Löhneisen, The metal-insulator transition in Si: P, *Festkörperprobleme* **30**, 95–111 (1990).

[157] D.V. Averin and K.K. Likharev, Coulomb blockade of single-electron tunneling, and coherent oscillations in small tunnel junctions, *J. Low. Temp. Phys.* **62**, 345–372 (1986).

[158] T.A. Fulton and G.J. Dolan, Observation of single-electron charging effects in small tunnel junctions, *Phys. Rev. Lett.* **59**, 109–112 (1987).

[159] D.V. Averin and K.K. Likharev, Single-electronics: a correlated transfer of single electrons and Cooper pairs in systems of small tunnel junctions, in *Mesoscopic Phenomena in Solids*, edited by B.L. Altshuler, P.A. Lee, and R.A. Webb (North-Holland, 1991), chap. 6.

[160] I.O. Kulik and R.I. Shekhter, Kinetic phenomena and charge discreteness effects in granulated media, *Sov. Phys. JETP* **41**, 308–321 (1975).

[161] L.J. Geerligs, M. Matters and J.E. Mooij, Coulomb oscillations in double metal tunnel junctions, *Physica B* **194–196**, 1267–1268 (1994).

[162] D.V. Averin, Periodic conductance oscillations in the single-electron tunneling transistor, *Physica B* **194–196**, 979–980 (1994).

[163] Y. Pashkin, Y. Nakamura and J. Tsai, Room-temperature Al single-electron transistor made by electron-beam lithography, *Appl. Phys. Lett.* **76**, 2256–2258 (2000).

[164] W.L. McMillan, Scaling theory of the metal-insulator transition in amorphous materials, *Phys. Rev. B* **24**, 2439–2443 (1981).

[165] J.G. Massey and M. Lee, Direct observation of the coulomb correlation gap in a nonmetallic semiconductor, Si:B, *Phys. Rev. Lett.* **75**, 4266–4269 (1995).

[166] J.G. Massey and M. Lee, Electron tunneling study of coulomb correlations across the metal-insulator transition in Si:B, *Phys. Rev. Lett.* **77**, 3399–3402 (1996).

[167] M. Lee, J.G. Massey, V.L. Nguyen and B.I. Shklovskii, Coulomb gap in a doped semiconductor near the metal-insulator transition: Tunneling experiment and scaling ansatz, *Phys. Rev. B* **60**, 1582–1591 (1999).